UNIVERSITÀ DEGLI STUDI DI PADOVA

DIPARTIMENTO DI INGEGNERIA INDUSTRIALE
CORSO DI LAUREA MAGISTRALE IN INGEGNERIA CHIMICA E DEI PROCESSI INDUSTRIALI

Tesi di Laurea Magistrale in
Ingegneria Chimica e dei Processi Industriali

Catalytic ethanol dehydration to ethylene in microreactor

Relatore: ***Prof. Paolo Canu***

Correlatori: ***Prof. Tapio Salmi***
Prof. Dmitry Murzin
Doc. Narendra Kumar

Laureanda: ROSSANA SUERZ

ANNO ACCADEMICO 2018 – 2019

Project developed in:
Laboratory of Industrial Chemistry and Reaction Engineering
Department of Chemical Engineering
Åbo Akademi University

A mio nonno,

per il mancato confronto
che avremmo amato.

Abstract

The aim of this thesis is to study the production of ethylene by dehydration of ethanol, which also leads to two main by-products: diethyl ether and acetaldehyde. This reaction represents a green way of obtaining this alkene since ethanol can be obtained from biomass. The reaction has been tested in a microreactor and products analysed with on-line gas chromatography, with three different catalysts – γ-alumina, H-Beta-38 and Sn-Beta-38, together with the uncatalysed reaction. Temperature and residence time effects have been studied.

The catalysts were characterized with different physico-chemical techniques, in order to correlate their characterization results with catalytic properties of catalyst coated microplates in ethanol dehydration reaction. SEM-EDX, TEM, nitrogen physisorption, FTIR-Pyridine and white light confocal microscopy were used for the physico-chemical characterizations. An ultrasound pretreatment was performed to study the stability of catalyst coating on the microplates.

Based on the ethanol dehydration experiments, H-Beta-38 catalyst coated microplate exhibited the highest production of ethylene. The fresh catalyst allowed complete conversion and 98 % selectivity towards ethylene, deactivating significantly after some hours.

The kinetic model describing the distribution of the products for the reaction catalysed by H-Beta-38 was assessed, relating the formation of ethylene and diethyl ether to the concentration of Brønsted and Lewis acid sites, respectively. Experimental data were adequately described by the proposed mechanism.

Limitations of this study are mainly related to the challenges of performing post-run analyses, because of a small amount of catalyst, and a need of the removing from the microplates. Moreover, the inlet flow of ethylene was not monitored, therefore an estimation of the inlet concentration was used.

This master thesis project has been performed during an Erasmus+ period at Åbo Akademi University, supervised by Professors Tapio Salmi, Dmitry Yu. Murzin and Docent Narendra Kumar, with the help of Professor Johan Wärnå, Dr Kari Eränen and Dr Atte Aho.

Table of contents

Introduction **1**

Chapter 1 Ethanol dehydration in catalyst coated microreactor **3**

1.1 Ethylene production 3

1.2 Catalysts 5

1.3 Microreactor technology 5

Chapter 2 Experimental and methods **9**

2.1 Catalyst preparation and coating 9

2.1.1 Metal modification 10

2.1.2 Coating procedure 10

2.2 Characterization 11

2.2.1 White light confocal microscopy 12

2.2.2 Catalyst adhesion 12

2.2.3 Scanning electron microscopy 13

2.2.4 Energy dispersive X-ray analysis 13

2.2.5 Transmission electron microscopy 14

2.2.6 Nitrogen physisorption 14

2.2.7 Fourier Transform Infrared Spectroscopy 15

2.3 Reaction set-up 16

2.3.1 Microreactor 17

2.3.2 Scheme of the system 18

2.3.3 Parameters 19

2.3.4 Gas chromatography 19

Chapter 3 Results **23**

3.1 Reaction 23

3.1.1 Uncatalysed reaction 24

3.1.2 Alumina 25

3.1.3 H-Beta-38 26

3.1.4 Sn-Beta-38 28

3.2 Characterization 31
3.2.1 Surface roughness 31
3.2.2 Coating adhesion, uniformity and stability 32
3.2.3 Crystal size distribution 34
3.2.4 Catalyst composition 35
3.2.5 Pore size distribution 36
3.2.6 Surface area 37
3.2.7 Acidity 37
3.3 Discussion 38
Chapter 4 Kinetics **39**
4.1 Reaction mechanism 39
4.2 Kinetic modelling 40
4.3 Reactor model 42
Conclusions **47**
Notation **51**
Appendix **53**
References **59**
Acknowledgements **63**

List of figures

1.1.	Main products from ethylene.	3
1.2.	Biomass-based routes to lower olefins.	4
1.3.	Reactor technology comparison.	7
2.1.	Calcination program used for NH_4-Beta-38 for obtaining its proton form.	9
2.2.	NanoFocus µSurf.	12
2.3.	LEO Gemini 1530.	13
2.4.	EOL JEM-1400Plus for TEM analyses.	14
2.5.	Sorptomatic 1900.	15
2.6.	ATI Mattson – Infinity Series.	16
2.7.	Schematic representation of the GPMR-Mix device: a) platelets disposition and b) indication of section of operation.	17
2.8.	Gas Phase Micro Reactor with Mixer and Internal Heating/Cooling.	17
2.9.	Photo of the reaction system, where it is possible to identify the bubbler, soaked in a bath with cooling water, and the microreactor housing.	18
3.1.	Effect of temperature and residence time on product distribution (a, c) and conversion and selectivity (b, d) for the uncatalysed reaction.	24
3.2.	Effect of temperature and residence time on product distribution (a, c) and conversion and selectivity (b, d) over γ-alumina.	25
3.3.	a) Product distribution and b) conversion and selectivity with time on stream over γ-alumina.	25
3.4.	Effect of temperature and residence time on product distribution (a, c) and conversion and selectivity (b, d) over H-Beta-38.	26
3.5.	a) Product distribution and b) conversion and selectivity on time on stream over H-Beta-38 catalyst.	27
3.6.	Dependence of conversion and selectivity for the fresh, spent and regenerated H-Beta-38 on a) temperature and b) residence time.	28
3.7.	Effect of temperature and residence time on product distribution (a, c) and conversion and selectivity (b, d) over Sn-Beta-38.	29

3.8.	a) Product distribution and b) conversion and selectivity with time on stream for ethanol transformation over Sn-Beta-38.	29
3.9.	Product distribution with time on stream during the a) first and b) second durability studies with Sn-Beta-38; c) corresponding conversion and selectivities.	30
3.10.	a) Visualization of a microchannel of a pristine plate and b) its surface roughness obtained by white light confocal microscopy	31
3.11.	a) Visualization of one microchannel of a calcined plate and b) its surface roughness obtained by white light confocal microscopy	32
3.12.	Scanning electron micrographs of a calcined plate: a) overview of the channel and b) its magnification.	32
3.13.	Scanning electron micrographs of the first plate obtained with H-Beta-38; a) overview of the channels and b) magnification of one of the spots were the catalyst is not attached.	33
3.14.	Scanning electron micrographs of the plates coated with a, b) γ-alumina, c, d) H-Beta-38 and e, f) Sn-Beta-38, fresh on the left, spent on the right.	33
3.15.	Scanning electron micrographs of the plates coated with a) γ-alumina, b) H-Beta-38 and c) Sn-Beta-38 and d) their corresponding crystal size distribution.	34
3.16.	Transmission electron micrographs of a) γ-alumina, b) H-Beta-38 and c) Sn-Beta-38 and d) their corresponding pore size distribution.	36
4.1.	Reaction network of ethanol dehydration over H-Beta-38.	39
4.2.	Model and experimental data profile of outlet concentration of ethanol.	44
4.3.	Model and experimental data profile of outlet concentration of ethylene.	45
4.4.	Model and experimental data profile of outlet concentration of diethyl ether.	45
A.1.	Schematic representation of the reaction system.	53
A.2.	Mass balance with time on stream over γ-alumina.	55
A.3.	Mass balance with time on stream over fresh H-Beta-38.	56
A.4.	Mass balance with time on stream over regenerated H-Beta-38.	56
A.5.	Mass balance with time on stream over fresh Sn-Beta-38.	57
A.6.	Mass balance with time on stream over regenerated Sn-Beta-38.	57

List of tables

2.1.	Calcination procedure used for the thermal pre-treatment of plates.	10
2.2.	pH values of the slurry mixtures prepared.	11
2.3.	Calcination program used for the coated plates. Values refer to the time needed to reach the corresponding temperature or to time the plates were kept at that temperature.	11
2.4.	Characteristic dimensions of the reaction plates.	18
2.5.	Retention time and response factors obtained for components analysed with GC.	21
3.1.	Results of EDX for H-Beta-38 and Sn-Beta-38.	35
3.2.	Values of specific surface area and micropore volume obtained with performing N_2 physisorption on the catalysts.	37
3.3.	Acid sites concentration of γ-alumina, H-Beta-38 and Sn-Beta-38 obtained by FTIR.	37
4.1.	Values of pre exponential factors A and activation energies Ea obtained by fitting.	46

Introduction

Facing with the increasing scarcity of petroleum resources, nowadays is becoming important, day by day, to find alternative ways of producing the commodities obtained, until now, by fossil oil processing.

Ethylene is the largest of the basic chemical building blocks, one of the most important raw materials in the petrochemical industry. The aim of this thesis is to find the conditions that lead to the highest productivity of ethylene from the dehydration of ethanol. From this reactant, two main by-products can be formed: diethyl ether and acetaldehyde.

It is known that ethanol dehydration to ethylene is promoted by acid catalysts. In this work, three catalysts have been considered: γ-alumina, H-Beta-38 and its tin modified form, Sn-Beta-38. Temperature and residence time studies, together with deactivation and regeneration studies, allowed to perform catalyst screening.

Catalysts have been characterized with different techniques: concentration of Brønsted and Lewis acid sites has been measured by FTIR using pyridine as a probe molecule, while specific surface area and pore volume was determined with nitrogen physisorption. SEM-EDX was used for the evaluation of the catalyst coating, obtained with a slurry deposition method, for retrieving the crystal size distributions on the microchannels, and for determination of the elemental composition of the catalysts, in particular for the calculation of the silica to alumina ratio. Pore size distributions have been measured by the transmission electron microscopy. The surface roughness of microchannels has been estimated by white light confocal microscopy.

Ethanol dehydration was performed at ambient pressure, in a gas phase microreactor (IMM). Ethanol was fed into the reactor through to a bubbling system, where helium was used as carrier gas. The outlet stream of the reactor is connected to an on-line gas chromatograph, from which it was possible to obtain, after calibration, the outlet concentration of products.

The reaction has been tested at different temperature and residence time with all catalysts; kinetic studies performed with the best one helped to define the mechanism of the reaction. The use of a microreactor enhances the kinetic studies: because of a high surface to volume ratio, mass transfer limitations are negligible, ensuring the kinetic control.

This thesis is divided into four chapters:

- Chapter 1 deals with a brief introduction about the state of art of ethanol dehydration, reporting the reactions that lead to product and by-products. A short overview of catalysts used is provided, and the microreactor technology, with its advantages and drawbacks, is outlined.

- Chapter 2 is a collection of experimental methods used for this project. Procedures used for the metal deposition and coating are explained, together with the analyses used for characterization of the microplates and catalysts. The reaction set-up is finally explained, underlying how parameters were changed during the experiments and how the products have been analysed.

- Chapter 3 groups all results obtained: products distributions of experiments performed in the microreactor, both with and without catalysts. Characterization data are listed and commented, and eventually, eventually, a correlation between the physico-chemical properties of the catalyst coated microplates and the catalytic behaviour in ethanol dehydration reaction is underlined.

- Chapter 4 deals with the kinetics of the reaction catalysed by H-Beta-38. Its mechanism is assessed and results of the simulation, performed with an optimization and parameter estimation software, are evaluated.

Chapter 1

Ethanol dehydration in catalyst coated microreactor

In recent years a need for substituting chemicals coming from fossil oil with biobased ones, because of the lack of petroleum resources has been recognized. Ethylene, widely used for plastics production, can be obtained by catalytic acid dehydration of ethanol, which in turn can be obtained by fermentation of sugars, such as agricultural wastes or lignocellulose.
Moreover, the use of microreactors allows performing a large number of experiments in a relatively short time, making understanding of the optimal reaction condition can be efficient.

1.1 Ethylene production

Ethylene $CH_2 = CH_2$ is the simplest alkene, used as a building block in the petrochemical industry, for the production of solvents, packaging, plastics, cosmetics, pneumatics and paints, as reported by Technip FMC (2017). The main products that can be obtained from ethylene are collected in Figure 1.1, showing a wide range of commodities.

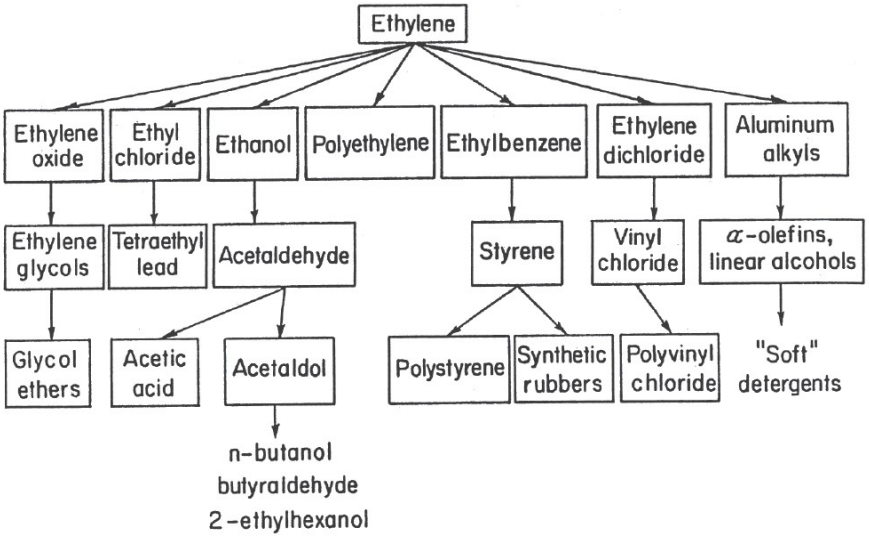

Figure 1.1. Main products from ethylene.

Ethene is commonly obtained by steam cracking of naphtha; this process involves fast, high-temperature reaction occurring in 0.1-0.6 s, at ca. 800 °C.

As Van Haveren *et al.* (2008) explained already a decade ago, there is limited success in finding new and easily accessible crude oil reservoirs, thus there is a perception that the era of cheap fossil oil is ending. A need for more sustainable production methods is every day becoming more relevant.

Eggersdorfer *et al.* (1992) reported that realistically the world biomass production is 170000 million tons/year, but only 3 % of it is being cultivated, harvested and used for human consumption (food and non-food). This means that biomass could be used as a source of energy and chemicals – whole-plant combustion, bioalcohol production and its use as gasoline for cars, or rape-seed oil and its methyl ester as fuel for diesel cars – without the risk of harming resources for human consumption.

Ethanol could be obtained by fermentation of biomass. Further reactions to olefins can be seen in Figure 1.2 (Okkerse and Bekkum, 1999). Mäki-Arvela *et al.* (2011) affirmed that bioethanol production by enzymatic fermentation of sugars is technology feasible having a large economic impact; already in 1946, Harris and Beglinger exposed a process for obtaining ethanol from agricultural wastes.

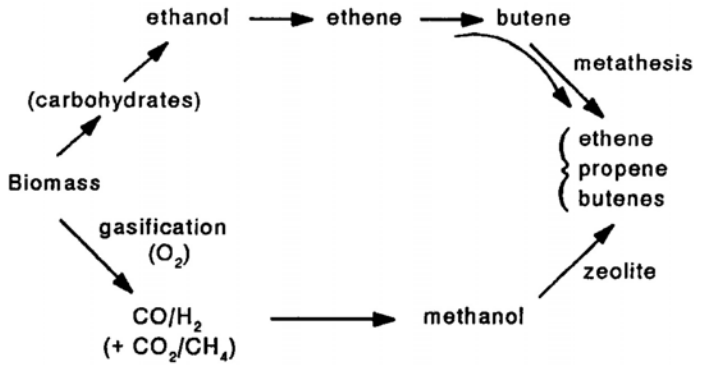

Figure 1.2. Biomass-based routes to lower olefins.

Ethylene is directly produced in nature during the ripening of fruits, for example, but the amount is so limited that an economical process may be practically impossible (van Haveren *et al.*, 2008). Dehydration of ethanol represents, therefore, one way for obtaining bio-based ethylene; the reaction is indicated in Equation (1.1).

$$C_2H_5OH \leftrightarrows C_2H_4 + H_2O \quad (1.1)$$

This is an endothermic reaction, with ΔH^0 (298 K) = +44.9 kJ/mol (Wu and Wu, 2017).

The main by-product of this reaction is diethyl ether, while small amounts of acetaldehyde and some hydrocarbons can be also generated (Zhang and Yu, 2013).

$$2\ C_2H_5OH \leftrightarrows (C_2H_5)_2O + H_2O \quad (1.2)$$

$$C_2H_5OH \leftrightarrows CH_3CHO + H_2 \quad (1.3)$$

Equations (1.2) and (1.3) describe the formation of the main by-products. Varisli *et al.* (2007) suggested that formation of ethylene is due to dehydraion of chemisorbed ethanol molecules, while the formation of diethyl ether is a result of a reaction between chemisorbed and physisorbed ethanol molecules on the catalyst surface.
Takahara *et al.* (2005), assuming that dehydration is catalysed by solid acid catalysts, investigated the effect of different zeolites and silica-alumina compounds and concluded that Brønsted acid sites, in particular strong ones, are responsible for dehydration of ethanol to ethylene.

1.2 Catalysts

Dehydration of ethanol is promoted by acid catalysts. The material chosen for this application H-Beta-38 is a microporous material, with a high surface area and a high concentration of Brønsted and Lewis acid sites. Jansen *et al.* (1997) reported that beta zeolites have Brønsted acid sites in the micropores and on the external surface, while the presence of Lewis acid sites is due to local defects on the internal surface.
Besides H-Beta-38, two other catalysts were considered, namely γ-alumina and Sn-Beta-38, allowing to study the influence of Brønsted acidity and the role of tin.
γ-alumina, bearing Lewis acidity, is often used as catalyst support (Paranjpe, 2017).
Tin promotes Lewis acid-catalyzed reactions and is believed to inhibit hydrocracking, isomerization and coke formation: these properties may lead to an enhancement of performances of the proton form of the zeolite.

1.3 Microreactor technology

According to Ehrfeld *et al.* (2006), microreactors usually are defined as miniaturized reaction system fabricated by using, at least partially, methods of microtechnology and precision engineering. Characteristic dimensions of the internal structures of microreactors like fluid channels typically range from the sub-micrometre to the sub-millimetre range.
Several advantages can be related to the use of smaller equipment, if compared to the laboratory scale ones (Ehrfeld *et al.*, 2006; Salmi *et al.*, 2011; Yue, 2018):

- saving of space, materials and energy;
- reduced response time;

- efficient heat transfer;
- sufficient mass transfer;
- high surface area-to-volume ratio;
- immobilization of the catalyst;
- isothermal conditions.

Salmi *et al.* (2011) underlined that microreactor technology enhances three of the basic necessities of chemical reactors: optimal reaction time, good and fast heat transfer in the reaction zone, and sufficient mass transfer.

The rapid heat and mass transfer of microreactors, which is due to a significantly high surface to volume ratio, leads to a significantly faster reaction with respect to batch reactors. Enhancement of the heat transfer prevents the hotspots that usually appear in batch systems. Having small volumes enables a safer use of highly toxic or explosive reactants, and strongly exothermal reactions can be cooled down rapidly. Microreactors usually work at high relative concentration of reactants, therefore volumes of solvents and bioproducts per unit of products are smaller and wastes are significantly reduced. Immobilization of the catalyst allows the microreaction technology to improve process control and reliability. In continuous operations there is no need for removal of the catalyst, leading to high product purity (Yue, 2018).

Few drawbacks should even be considered:

- small volumes mean that there is usually laminar flow (mixing under diffusion control);
- risk of fouling;
- small productivity.

Together with this, it must be even considered that because of the small flowrates, the concentrations have a smaller order of magnitude with respect to conventional reactors, which means that relative error on data analysis is higher and that it is difficult to maintain constant flows. Small oscillations influence quite significantly the final value of inlet concentrations. Moreover, because of the low amounts of catalysts used in microreactors, post-run analysis is trivial. Most characterization techniques require a certain amount of catalyst to be performed, which is usually far from the quantities used for these applications. In particular, with coated microreactors, the catalyst should be scratched from the microplates.

Despite these drawbacks, microreactors proved to be optimal for laboratory studies. Reactions taking place in them are kinetically controlled; there are no mass and heat transfer limitations – see Figure 1.3, and mixing is efficient.

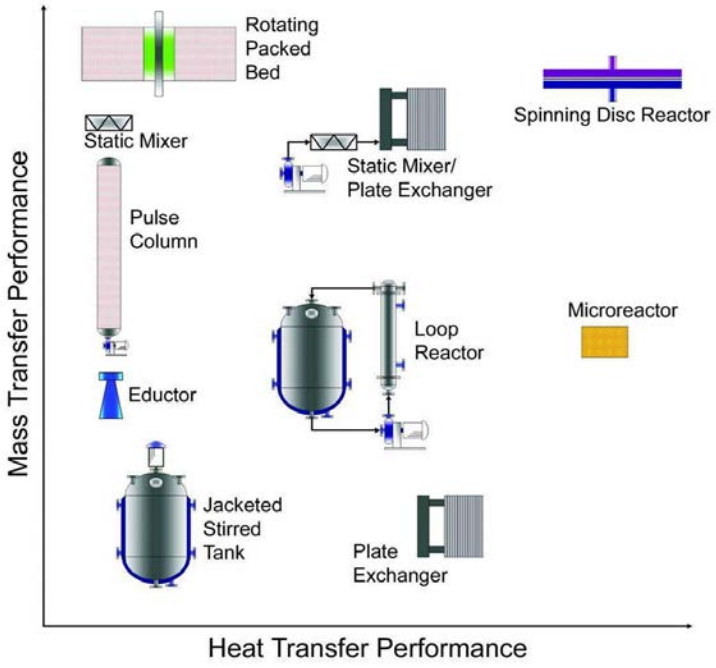

Figure 1.3. Reactor technology comparison (Hall and Stocker, 2003).

Small amounts of reactants are required, and the response time is short: catalyst screening, for example, can be very fast – a large number of experiments can be performed in a shorter time scale (Salmi *et al.*, 2011).

On the other hand, it is not inconceivable to think about extending the microreactor technology to larger-scale production. The IMM Catalogue (2017) reported that production capacity in microreactors can reach 100 tons/year. The use of such reactors is mainly intended for manufacture of drugs and fine chemicals rather than for bulk chemical production.

In addition, higher production rates can be obtained by scaling up, which in case of microreactors is numbering-up: reactors are used in parallel instead of increasing their dimensions. The latter would lead to the loss of their advantages, such as absence of heat and mass transfer limitations. Numbering up may not be always the best choice in terms of costs, giving substantial advantages in terms of process control for reactions involving hazardous components.

Microreactor technology offers eventually a possibility of decentralized production (Salmi *et al.*, 2011), substituting the need for large production facilities.

Chapter 2

Experimental and methods

This chapter deals with the description of the experimental work performed and of the physico-chemical analysis used for characterization. Three different catalysts have been considered: γ-alumina, H-Beta-38 and Sn-Beta-38. The latter obtained by Sn modification on the H-Beta-38 zeolite using evaporation impregnation catalyst synthesis method. Coating has been performed through the slurry deposition method and several analyses have been performed for characterization of pristine and coated microplates, and the powder form of catalysts.
The following analysis was done in this chapter: with light confocal microscopy for surface roughness studies; ultrasound testing to judge the quality of the coating; SEM for calculating the crystal size distribution; EDX for elucidation of catalyst composition; TEM to calculate the pore size distribution; N_2 physisorption for the specific surface area and pore volume. FTIR using pyridine as a probe molecule was used for the measurements of the amount of Brønsted and Lewis acid sites in the γ-alumina, H-Beta-38 and Sn-H-Beta-catalysts..

2.1 Catalyst preparation and coating

The catalyst supports used for coating of micro-plates were γ-alumina (Sasol-Disperal) and H-Beta-38 (Zeolyst International). The NH_4-Beta-38 was transformed to H-Beta-38 using the step calcination procedure illustrated in Figure 2.1.

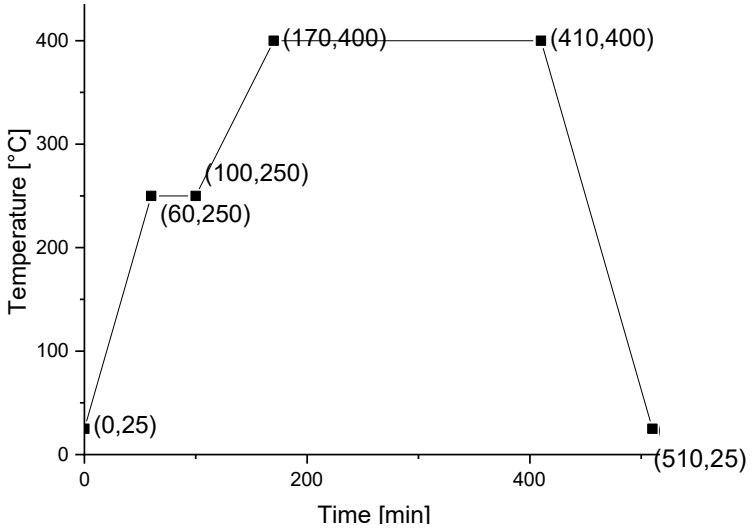

Figure 2.1. Calcination program used for NH_4-Beta-38 for obtaining its proton form.

Sn-H-Beta-38 zeolite catalyst was obtained by modification of H-Beta-38 using an aqueous solution of $SnCl_2$. The method of Sn modification used was evaporation impregnation. Coating of the microplates was achieved from the corresponding suspensions.
Microreactor plates were thermally pre-treated prior to the coating with the step calcination procedure described in Table 2.1.

Table 2.1. Calcination procedure used for the thermal pre-treatment of plates.

t [min]	T [°C]
75	250
60	250
85	750
180	750
100	25

This method, based on the results obtained by Zhang (2011), allows to increase significantly the surface roughness of the plates, which is fundamental for the catalyst adhesiveness.

2.1.1 Metal modification

Sn-modified H-Beta-38 catalyst was synthesized using evaporation impregnation method. The reason for the selection of this method is that it allows high dispersion of tin metal particles without influencing the structure of H-Beta-38 zeolite catalyst.
3.5 g of stannous chloride[1] have been dissolved in 250 mL of distilled water. 10 g of H-Beta-38 were added to the solution, which was placed in a round flask, soaked in a silicon oil bath for 24 h at 60 °C, rotating at 50 rpm. The catalyst was then extracted through vacuum evaporation, at 50 °C using the same rotational speed. After ca. 1 hour the dry catalyst was then placed in an oven for 7 h at 100 °C for further drying. Sn-Beta-38 was finally obtained with the following step calcination procedure: constant heating for 85 min up to 200 °C; after 65 min at this temperature, ramping to 425 °C in 45 min and holding for 180 min. Ambient temperature has been eventually reached in 100 min.

2.1.2 Coating procedure

Catalyst coating on microplates can be difficult, due to the characteristic dimensions of the latter. The slurry deposition method was, therefore, selected because of its flexibility.
According to Schmidt (2014), the catalyst was sieved in order to obtain a particle size below 32 μm. 0.17 g of the sieved powder was added to 5 mL of distilled water. Because of the acidic catalysts used, the pH of the mixture was always below 5. Therefore, some drops of ammonia

[1] $SnCl_2$, anhydrous, minimum 99%, Sigma-Aldrich.

solution[2] (NH_4OH, 32 %) were added in order to obtain pH ≅ 8.8. According to Meille *et al.* (2009) the acid may participate in the disaggregation of large particles, forming colloids and thus the gel solution. To avoid this, the pH is increased. Actual values of pH obtained in the slurries are listed in Table 2.2.

Table 2.2. pH values of the slurry mixtures prepared.

	pH [-]	
Catalyst	**With water**	**After ammonia addition**
Alumina	4.0	8.9
H-Beta-38	4.4	8.5
Sn-Beta-38	3.5	9.0

Once ready the mixture was stirred with a magnetic stirrer at 250 rpm, first at 50 °C for 4 h, and then for 2 days at room temperature. Deposition on the microplates of ca 3 μL of the suspension was done using a Finnpipette (0.5-5 μL). After placing microplates in a fridge at 5 °C for slow drying for 7 hour; the excess of catalyst, located outside the channels, was scratched away with a plastic spoon. Coated microplates were therefore placed in the oven at 110 °C for 7 h for further drying. The fridge dried catalyst coated microplates were calcined in a muffle oven using the step calcination procedure indicated in Table 2.3.

Table 2.3. Calcination program used for the coated plates. Values refer to the time needed to reach the corresponding temperature or to time the plates were kept at that temperature.

Alumina		**H-Beta-38**		**Sn-Beta-38**	
t [min]	**T [°C]**	**t [min]**	**T [°C]**	**t [min]**	**T [°C]**
70	250	60	250	70	250
50	250	45	250	60	250
45	400	65	550	50	400
180	400	180	550	180	400
100	25	100	25	100	25

Temperatures were reached slowly in order to avoid the formation of fractures, both in the plates and in the catalyst.

2.2 Characterization

One of the main tasks with catalytic application is to correlate their physical and chemical properties with catalytic behaviour; for this reason, several analyses have been performed. White light confocal microscopy was used to calculate the surface roughness of the microplates and ultrasounds helped to understand how good the adhesion of the catalysts was; SEM-EDX

[2] EMPLURA®, Ammonia solution 32%, Merck.

and TEM analysis were performed. Finally, the nitrogen physisorption analysis was used for calculating the surface area and pore volume and acidity measurements have been achieved with FTIR using pyridine as a probe molecule.

2.2.1 White light confocal microscopy

The white light confocal microscope is a powerful instrument for fast and accurate three-dimensional measurements of the surface topography (Jordan, 2001). This microscope works in the conventional range of magnification of optical microscopy; it is built as transmission microscopy with an enlightened system superimposed to it. This illuminates the sample and takes different images at different heights, which are processed and give 3D images.

Figure 2.2. NanoFocus μSurf.

Figure 2.2 shows the NanoFocus μSurf used to evaluate the surface texture and roughness of the microchannels. Results can be investigated both by images of the samples and by the arithmetical mean height *Sa* and the root mean square height *Sq*, provided by the analyser.

2.2.2 Catalyst adhesion

Once the plates have been coated, it is important to understand if the catalyst is sufficiently adhering to the channels or not. For this reason, once the coating procedure was completed, one of the coated plates was placed in a round flask and immersed in a water bath for an ultrasound stability test. This was performed for 4 hour, with the frequency f = 50 Hz and the power P = 70 W.

Therefore, it was possible to observe if the catalyst was detached from the plates. Further confirmation about the stability of catalyst coating was performed by characterization of the ultrasound treated H-Beta-38, Sn-H-Beta and alumina catalyst coated microplates using scanning electron microscopy.

2.2.3 Scanning electron microscopy

Scanning electron microscopy is described by Grasserbauer *et al.* (2009) as an analytical technique where secondary electrons are generated by an electron source, commonly a tungsten filament, which undergoes energy exchange with the sample, leading to inelastic scattering as well as the emission of secondary electrons and X-ray. The electrical signal resulting is amplified and translated to pixels (Egerton, 2005), providing a high resolution and high depth of field black and white images.

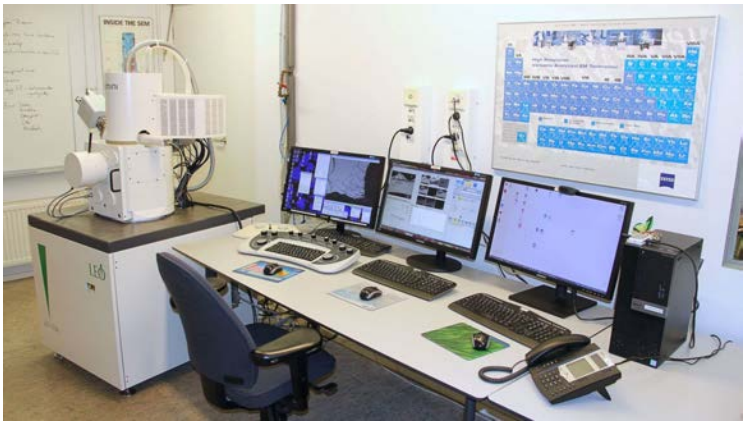

Figure 2.3. LEO Gemini 1530.

The analysis was performed using LEO Gemini 1530, in Figure 2.3, with a Thermo Scientific UltraDry Silicon Drift Detector. The SEM was manufactured in Oberkochen, Germany, in 2001 by LEO, that has been bought by Carl Zeiss (Silvander). The lightest detectable element is beryllium for the Thermo Scientific UltraDry detector. SEM is equipped with a secondary electron, a backscattered electron and an In-Lens detector. The magnification of the image corresponds to a Polaroid 545 print with the image size of 8.9x11.4 cm.
Scanning electron microscopy was used to study the morphology, uniformity and thickness of the catalyst coated microplates. The equipment was also used for studying the stability of catalyst coating in the microplates. The crystal size distribution of the catalyst coated microplates was carried out using J-Image Program.

2.2.4 Energy dispersive X-ray analysis

In the scanning electron microscope, the X-ray emissions spectra given by scattered and unscattered electrons are recorded with a Si-Li diode in the energy-dispersive mode. These can be used for analytical analysis. EDX is also able to detect metal particles that are too small to be detected by images obtained with other analyses, e.g. SEM (Ertl *et al.*, 1997). This analysis can provide a quantitative estimate of the elements present in a sample as the ratio of

concentrations because the area of each peak is related to the number of X-ray photons contributing to it (Egerton, 2005).
Analyses have been performed with the SEM machine, with an X-ray detector manufactured by Thermo Scientific.
The elemental compositions of the powder Sn-H-Beta-38, H-Beta-38, γ-alumina and catalyst coated microplates were determined using energy dispersive X-ray analyses. The SiO_2/Al_2O_3 ratio of H-Beta-38 zeolite catalyst was also calculated using energy dispersive X-ray analyses.

2.2.5 Transmission electron microscopy

In comparison with optical microscopy, using optical lenses, transmission electron microscopy uses electro-magnetic ones for focusing an electron beam on the sample (Zhen and Zaera, 2006). Electrons passed through a thin specimen form a transmission electron diffraction pattern, which can be focused and imaged (Egerton, 2005). Electrons behave like negatively charged particles: they are deflected by electric or magnetic fields. Resolution of TEM is higher than SEM. The transmission electron microscopy was used to measure the Sn metal particles size and distributions in the powder form of Sn-H-Beta-38 catalyst. The textural properties such as pore size, the shape of pores, periodicity of pores and channel system of the catalysts were also studied.

Figure 2.4. EOL JEM-1400Plus.

Analysis has been conducted in collaboration with Turku University, where EOL JEM-1400Plus is available, displayed in Figure 2.4.

2.2.6 Nitrogen physisorption

Physisorption is a general phenomenon that occurs when a gas is brought into contact with a solid surface (Ertl *et al.*, 1997), involving different forces as the London dispersion and the

short-range intermolecular repulsion. Equilibrium pressure, temperature and nature of the gas-solid system influence the amount of gas adsorbed.

The relationship between the amount of adsorbed gas and the equilibrium pressure at a known temperature can be evaluated by the adsorption isotherm. Its shape allows to identify the qualitatively the surface area and the pore size distribution. It is then possible to evaluate them quantitatively, by different methods. The Brunauer-Emmett-Teller (BET) can be used for non-porous materials, while the Dubinin method is recommended for microporous materials (Rouquerol *et al.*, 2009). The nitrogen physisorption method was used to determine the surface area, pore volume, pore size distributions and adsorption-desorption isotherms. The surface area of the H-Beta-38, Sn-H-Beta catalysts were calculated using Dubinin's method and pore volume using Horvath and Kawasaki method.

Figure 2.5. Sorptomatic 1900.

Nitrogen has been used as adsorptive gas, being suitable for a large range of porous materials. The equipment used for the analysis was Sorptomatic 1900 by Carlo Erba Instruments (Figure 2.5).

2.2.7 Fourier Transform Infrared Spectroscopy

According to Ertl *et al.* (1997), infrared spectroscopy has proved to be the most powerful method for investigating into acid-base interactions on solid surfaces by using probe molecules like pyridine or carbon dioxide. This allows to distinguish Brønsted and Lewis acidity. Infrared spectroscopy is a technique where an infrared photon is adsorbed by a molecule, resulting in

vibrations of the chemical bonds. Visible for in this technique are only vibrations which lead to a change in the dipole moment. Mass of a molecule and the bond strength thereby mainly determine the energy needed to excite a bond.
Fourier transform infrared spectroscopy is performed with the aid of an interferometer, which transforms a spectrum from the frequency's domain to the time one; this allows reducing the frequency and thereby detection by normal detectors. It is, therefore, possible to obtain a graph representing how the power of the source changes with time, which is at the end taken back to the frequency domain by the Fourier transform.

Figure 2.6. ATI Mattson – Infinity Series.

The measurement of the amount of Brønsted and Lewis acid sites in the Sn-H-Beta-38, H-Beta-38 and Al_2O_3 catalysts was carried out by FTIR using pyridine as a probe molecule. Results obtained using the machine ATI Mattson – Infinity Series (Figure 2.6) were interpreted using the method developed by Emeis (1993). Catalysts were pressed into thin disks in order to perform the analysis.

2.3 Reaction set-up

The ethanol dehydration was used as a test reaction for the evaluation of the catalytic properties of Sn-H-Beta-38, H-Beta-38 and γ-Al_2O_3 catalyst coated microplates. The influence of temperature and residence on the conversion of ethanol and selectivity to desired products were studied. Experiments have been performed using a gas phase microreactor provided by IMM, where ethanol was evaporated by helium through a bubbling system: a mixture of the two gases flowed in the reactor and products were analysed with an on-line gas chromatograph. The range of temperature considered for the catalysed reactions was between 225 °C and 325 °C, while without catalyst ethanol dehydration has been performed up to 400 °C. The residence time ranged between 0.013 s and 0.030 s.

2.3.1 Microreactor

The microreactor device has been provided by the Institute für Mikrotechnik Mainz GmbH (IMM). The gas-phase microreactor with a mixer and the internal heating/cooling GPMR-MIX -002 contains two cavities, each filled with one stack of microstructured platelets; two pipes allow the inlet (IMM-Catalogue, 2017).

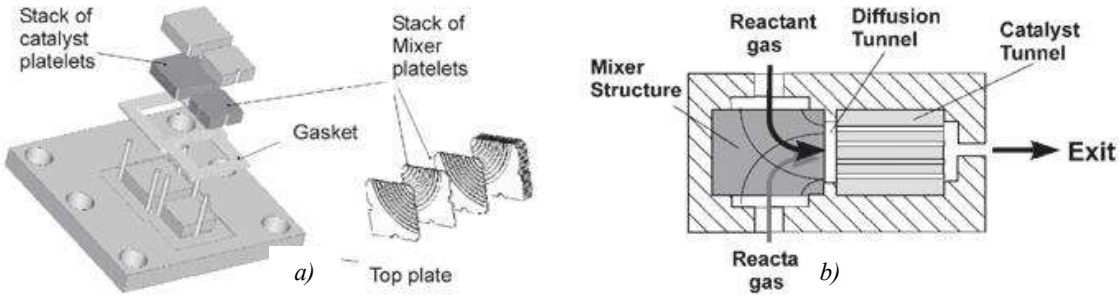

Figure 2.7. Schematic representation of the GPMR-Mix device: a) platelets disposition and b) indication of section of operation (IMM Catalogue, 2017).

Figure 2.7 provides a schematic representation of the microreactor showing how microplates are arranged on their housing plate. The reactor has ten platelets of each type. Figure 2.7.b shows the inlet, outlet and reaction sections.

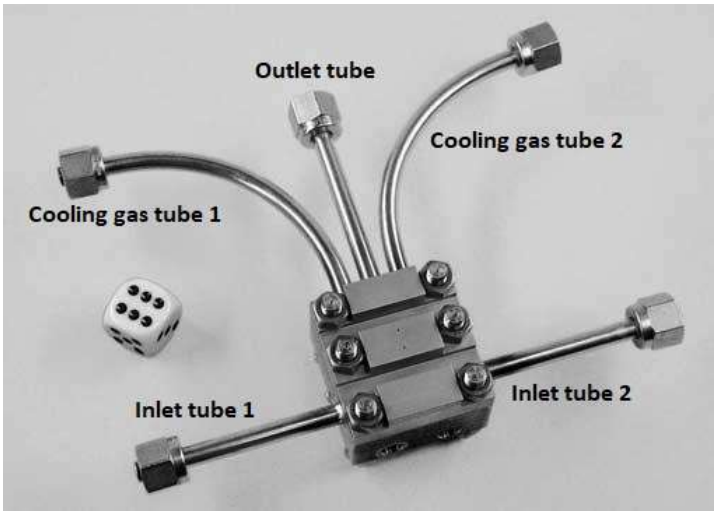

Figure 2.8. Gas Phase Micro Reactor with Mixer and Internal Heating/Cooling (IMM Catalogue, 2017).

The shell of the reactor could be observed in Figure 2.8, where all connection streams are indicated for better understanding of the system.

Table 2.4. Characteristic dimensions of the reaction plates.

Unit	Values
Plate [mm×mm]	9.5×9.5
Channel width [μm]	460
Channel depth [μm]	125
Specific surface area per reaction layer [m^2/m^3]	3840
Active inner volume per layer [mm^3]	2.5

Characteristics dimensions of the reaction microplates are listed in Table 2.4 corresponding to the actual reaction section.

2.3.2 Scheme of the system

The inlet flow was a mixture of helium and ethanol. The reactant was placed as a liquid in a bubbling system at ambient temperature. Helium was pumped[3] into the bubbler and used as a carrier gas. This mixture then flowed into the reactor, which was heated with a programmable temperature controller (CAL 9500P). The outlet line was quenched at 150 °C by CAL 3300, in order to stop the reaction, and connected to a gas chromatographer for online analysis.

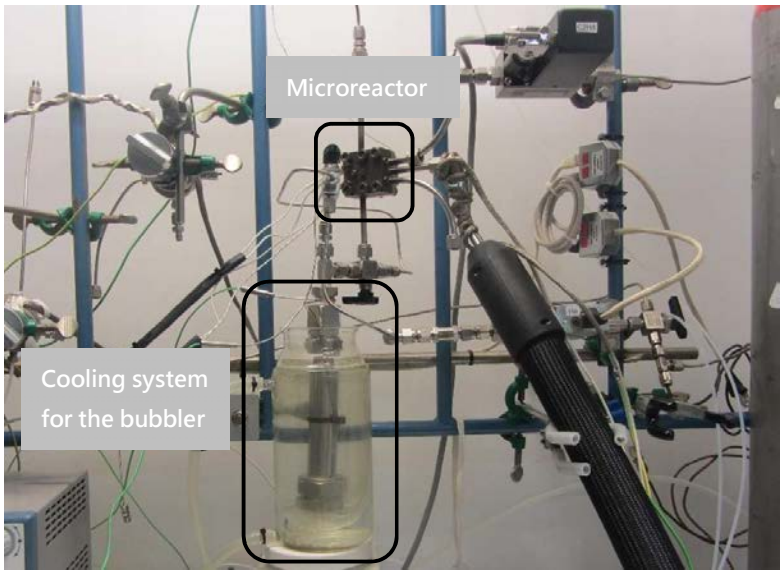

Figure 2.9. Photo of the reaction system, where it is possible to identify the bubbler, soaked in a bath with cooling water, and the microreactor housing.

Figure 2.9 depicts the reaction system: the bubbling system, on the left, was kept at 25 °C by a thermostat; the thermocouples were connected to the external wall of the bubbler and to the microreactor for continuously monitoring the temperature. Inlet lines of the microreactor were connected to the bubbler and with an ethylene bottle, used for calibration of the gas

[3] Bronkhorts high-tech.

chromatograph, as explained in §2.3.4. The outlet line was connected to the analysis system and to the fume.

2.3.3 Parameters

The reaction has been tested changing three different parameters: catalyst, temperature and residence time. Effect of temperature and residence time on products distribution have been studied for each catalyst, and the same procedure has been followed for not coated plates.
Temperature has been studied in the range between 225 °C to 325 °C for the catalysed reactions. The lower limit was defined from the formation of ethylene, while 325 °C were never exceeded in order to avoid changes in the structure of the catalysts and to avoid non catalytic thermal reactions, which became particularly relevant above 350 °C.
The residence time effect is driven by the operating range of the pump used for helium; this has been used from 2 mL/min to 4.5 mL/min, corresponding to the residence time from 0.013 s to 0.030 s. Smaller flow rates have not been considered, because of the flow instability at these rates, while larger ones would have led to low conversions.
Deactivation was also taken into consideration: catalysts durability studies were performed for several days, flowing continuously the mixture of ethanol and helium and analysing changes in the product distribution. The effect of residence time and temperature was studied for the deactivated catalyst, as well as after regeneration.
Regeneration was performed at 400 °C for 4 h, flowing 3 mL/min of synthetic air[4] in the reactor.
All experiments were conducted at ambient pressure.

2.3.4 Gas chromatography

Outlet streams of the reactor were analysed with online gas chromatography – Agilent Technologies, 7820A GC System.
Gas chromatography is a separation technique for mixtures using the distribution equilibria of the analytes between a stationary (solid/liquid) and a mobile phase (gas).
Gas chromatography is a quantitative analysis, which does not provide direct information about the structure of the analyte; it is necessary to identify at first the products and the reference factors that allow obtaining the concentrations of the products.
Calibration was, therefore, performed using ethylene as a reference. At first, a constant and known flowrate was introduced in the microreactor together with helium, and the retention time and the area of the peak at that concentration of ethylene were obtained. Then, the same flowrate of helium was passed through the bubbling system and ethanol was withdrawn. The area of the peaks is proportional to their concentration:

[4] 20% O_2, 80% N_2

$$c_{C_2H_4,1}: A^{GC}_{C_2H_4,1} = c_{C_2H_4,2}: A^{GC}_{C_2H_4,2} \tag{2.1}$$

No reaction was involved during the calibration, thus for the ideal gas one, where density is constant; the concentration can be written as in (2.2); Equation (2.1) can then be rearranged as (2.3)

$$c_{C_2H_4,i} = \frac{\dot{n}_{C_2H_4,i}}{\dot{V}_{Tot,i}} \tag{2.2}$$

$$\frac{\dot{n}_{C_2H_4,2}}{\dot{V}_{Tot,2}} = \frac{A^{GC}_{C_2H_4,2}}{A^{GC}_{C_2H_4,1}} \cdot \frac{\dot{n}_{C_2H_4,1}}{\dot{V}_{Tot,1}} \tag{2.3}$$

The flowrate of ethylene was not changed during the calibration, therefore:

$$\dot{n}_{C_2H_4,1} = \dot{n}_{C_2H_4,2} \tag{2.4}$$

The total flow was obtained rearranging Equation (2.4):

$$\dot{V}_{Tot,2} = \dot{V}_{Tot,1} \cdot \frac{A^{GC}_{C_2H_4,1}}{A^{GC}_{C_2H_4,2}} \tag{2.5}$$

The difference between the two volume flows obtained corresponds to the volume of ethanol withdrawn by helium, from this it is therefore possible to calculate the corresponding molar flow, using the hypothesis of an ideal gas – Equation (2.6).

$$\dot{n}_{C_2H_5OH,2} = \frac{P \cdot \dot{V}_{C_2H_5OH,2}}{R \cdot T} \tag{2.6}$$

From the molar flow, it was then possible to calculate the concentration of ethanol – Equation (2.7) – corresponding to the peak obtained by the GC. The reference factor was calculated as in (2.8).

$$c_{C_2H_5OH,2} = \frac{\dot{n}_{C_2H_5OH,2}}{\dot{V}_{Tot,2}} \tag{2.7}$$

$$RF_{C_2H_5OH} = \frac{c_{C_2H_5OH,2}}{A^{GC}_{C_2H_5OH,2}} \tag{2.8}$$

The same calibration has been performed for diethyl ether, placing it in the bubbler instead of ethanol, while the response factor of ethylene was calculated from the peak since its molar and volume flow are known. The temperature in the reactor was set to 50 °C during these calibrations.

The response factor of acetaldehyde was calculated from the relative response factor values retrieved from literature, as indicated in Equation (2.9).

$$\mathrm{RF}_{\mathrm{CH_3CHO}} = \mathrm{RF}_{\mathrm{C_2H_5OH}} \cdot \frac{0.5}{0.75} \tag{2.9}$$

Placing acetaldehyde in the bubbling system in the same way as two other products was not possible because of a low boiling point of this compound (20.8 °C). Therefore, values from the literature were used following the same path as Equation (2.9).

Table 2.5. Retention time and response factors obtained for components analysed with GC.

Component	Retention time [min]	Reference factor [mol/L·pA·s]
Ethylene	4.8	$2.15 \cdot 10^{-10}$
Diethyl ether	5.7	$2.85 \cdot 10^{-10}$
Acetaldehyde	6.5	$1.35 \cdot 10^{-10}$
Ethanol	12.0	$2.03 \cdot 10^{-10}$

The final values of the response factors obtained are listed in Table 2.5, together with the retention time measured for each component. The retention time of acetaldehyde has been observed injecting the pure component in the GC.

Chapter 3

Results

In this chapter, the obtained results are collected. Product distributions, conversion and selectivities are reported for the studied catalysts, in the investigated range of temperature and residence time. Physico-chemical characterization results for catalysts and microplates are listed. Finally, the results are analysed and a correlation between the ethanol dehydration reaction trends and physico-chemical characterization properties of catalysts are evaluated.

3.1 Reaction

Kinetic results have been evaluated based on conversion and selectivity, calculated with Equations (3.1) and (3.2).

$$X = \frac{c^{\text{in}}_{\text{C}_2\text{H}_5\text{OH}} - c^{\text{out}}_{\text{C}_2\text{H}_5\text{OH}}}{c^{\text{in}}_{\text{C}_2\text{H}_5\text{OH}}} \tag{3.1}$$

$$S_{\text{i}}^{\text{C}_2\text{H}_5\text{OH}} = \frac{c^{\text{out}}_{\text{i}}}{c^{\text{in}}_{\text{C}_2\text{H}_5\text{OH}} - c^{\text{out}}_{\text{C}_2\text{H}_5\text{OH}}} \cdot \frac{\nu_{\text{C}_2\text{H}_5\text{OH}}}{\nu_i} \tag{3.2}$$

Conversion and selectivity were calculated from concentrations assuming the constant density. The inlet flow to the reactor mainly contained helium (ca. 0.95 v/v), therefore changes in the volume flows have been neglected.
The inlet concentration of ethanol was calculated from the outlet ones, according to Equation (3.3).

$$c^{\text{in}}_{\text{C}_2\text{H}_5\text{OH}} = c^{\text{out}}_{\text{C}_2\text{H}_5\text{OH}} + 2 \cdot c^{\text{out}}_{(\text{C}_2\text{H}_5)_2\text{O}} + c^{\text{out}}_{\text{C}_2\text{H}_4} + c^{\text{out}}_{\text{CH}_3\text{CHO}} \tag{3.3}$$

The inlet concentration was at first assumed constant, however because of the bubbling system, small changes in the cooling water bath temperature and coke formation, feed fluctuations were quite relevant, as concentrations are in the order of 10^{-7} mol/L. For the sake of simplicity, the inlet concentration is, therefore, obtained by the mass balance, which was checked for each experiment performed. The results are collected in the Appendix A.2.

3.1.1 Uncatalysed reaction

Ethanol dehydration has been tested without any catalyst, in order to understand how temperature and residence time affect the product distribution. The effect of temperature was studied with a helium flow of 3 mL/min, corresponding to a residence time of 0.018 s. The results are represented in Figures 3.1.a and 3.1.b: at the lowest temperatures, a small amount of ethanol is reacting, with conversions slightly exceeding zero. Upon increasing temperature, the conversion started to increase, together with selectivity, until reaching ca. 80 % for both X and $S_{ethylene}$, at 400 °C, the highest temperature tested. What is possible to observe, therefore, is that both conversion and selectivity are exponentially proportional to temperature.

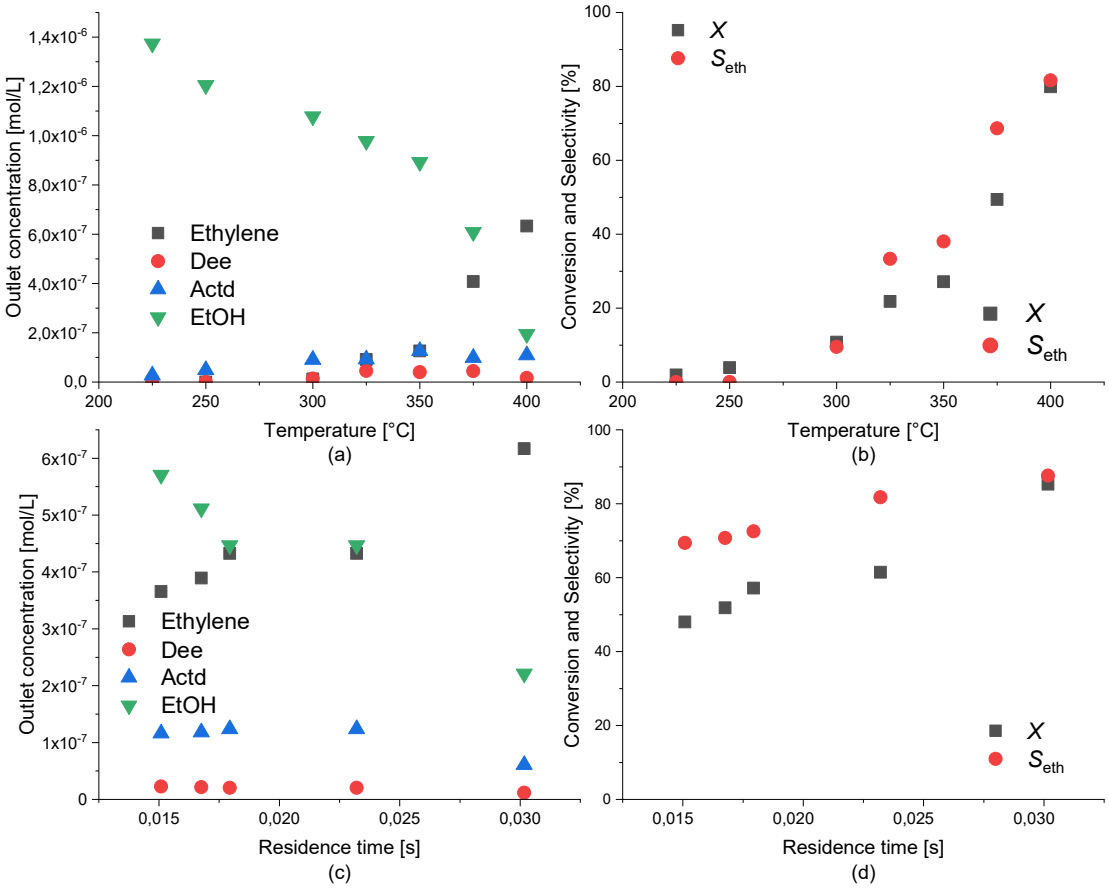

Figure 3.1. Effect of temperature and residence time on product distribution (a, c) and conversion and selectivity (b, d) for the uncatalysed reaction.

The same plots have then been represented to evaluate the effect of residence time - Figure 3.1.c and 3.1.d. Experiments have been performed at 400 °C. From these plots, it is possible to evaluate that even in this case conversion and selectivity are proportional to the residence time. Looking at the product distribution it is possible to observe that ethylene is the most abundant product; a low amount of acetaldehyde is produced, while diethyl ether formation is negligible.

3.1.2 Alumina

The temperature and the residence time effect has been tested for the γ-alumina catalysed reaction. Results are presented in Figure 3.2.

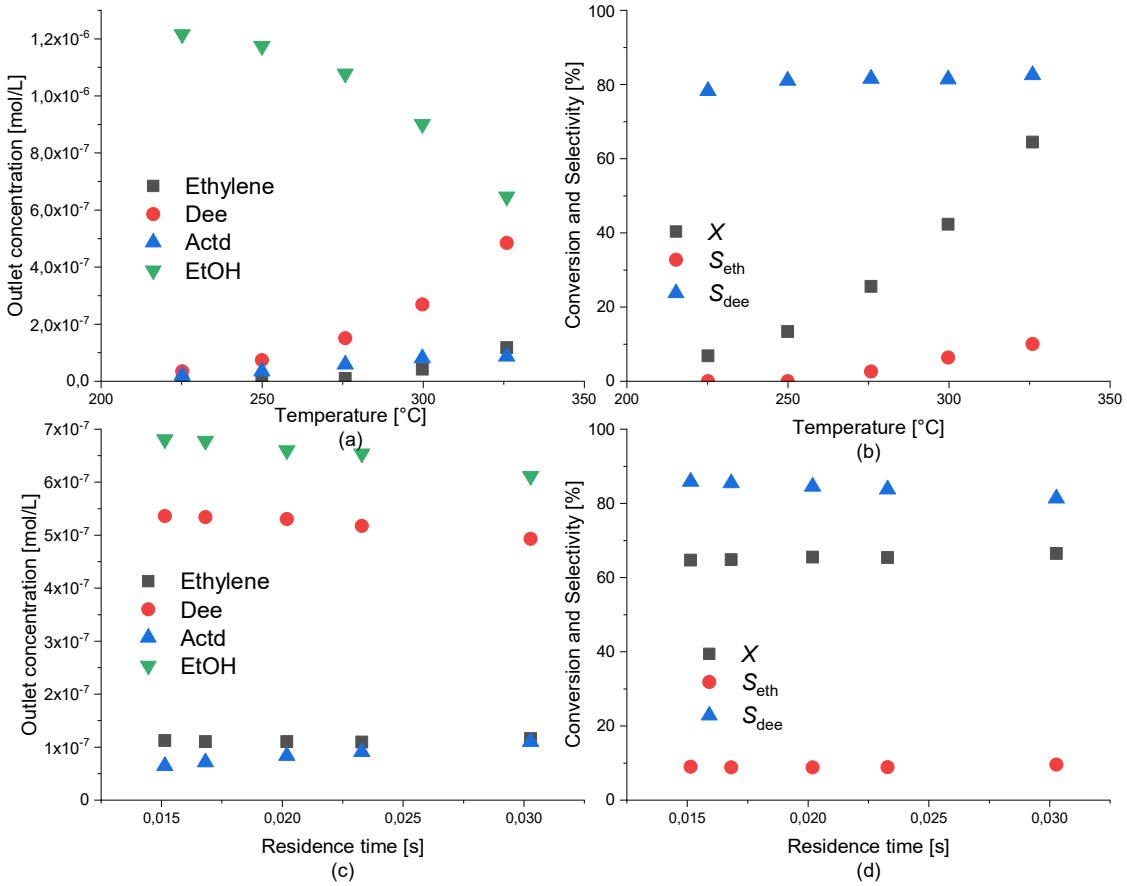

Figure 3.2. Effect of temperature and residence time on product distribution (a, c) and conversion and selectivity (b, d) over γ-alumina.

The main product observed with alumina is diethyl ether, showing increased selectivity with increased temperature.

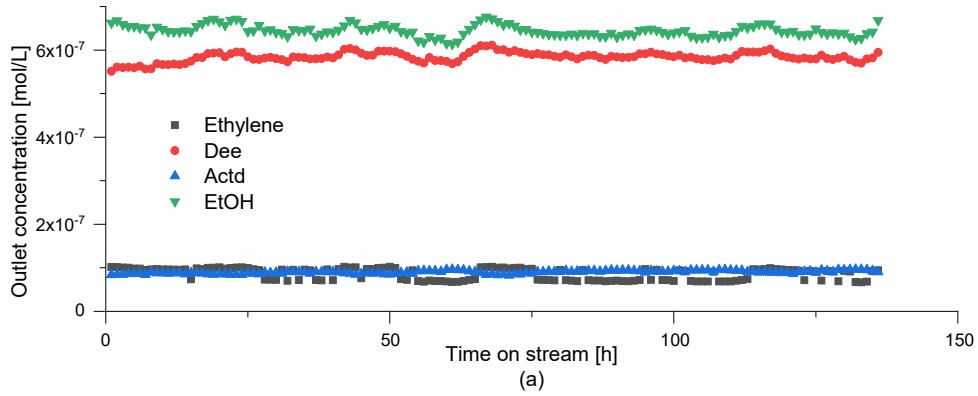

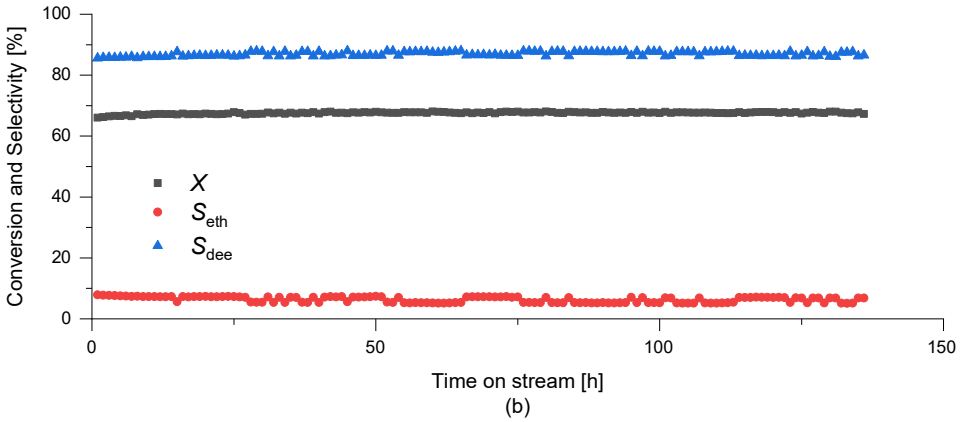

Figure 3.3. a) Product distribution and b) conversion and selectivity with time on stream over γ-alumina.

Stability of the catalyst was evaluated running the reaction for several days at 325 °C. As displayed in Figure 3.3, product distribution, conversion and selectivity were constant for several days, meaning that the catalyst did not deactivate.

3.1.3 H-Beta-38

The beta zeolite microplates underwent the same experiments as with γ-alumina, in order to understand how the presence of Brønsted acid sites influences the reaction. The temperature and the residence time have been exploited in the ranges explained in §2.3.3; the results are presented in Figure 3.4.

It can be clearly observed from Figure 3.4 that ethylene is the main product, which production increases significantly with temperature. Similar behaviour was noticed upon increase of the residence time. Conversion and selectivity towards ethylene are almost 100 %.

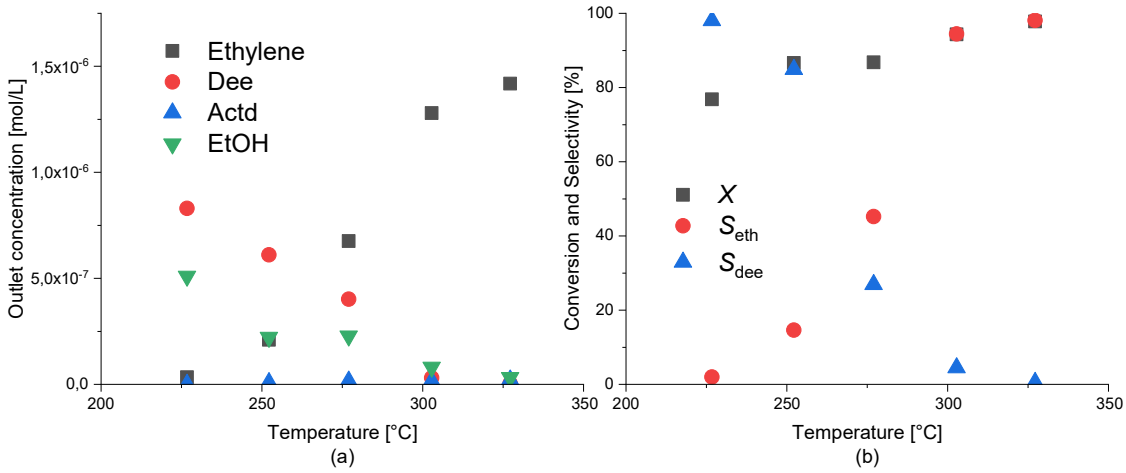

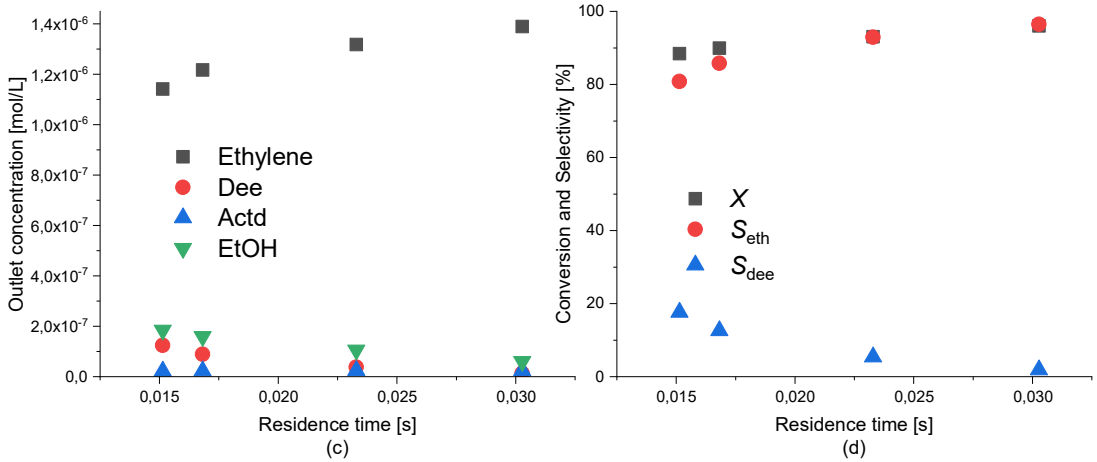

Figure 3.4. Effect of temperature and residence time on product distribution (a, c) and conversion and selectivity (b, d) over H-Beta-38.

Long-term stability was run for several days. In 6 days, the catalyst deactivated slowly, as displayed in Figure 3.5. Selectivity changed significantly, and diethyl ether, became the main product already after the first 24 hours.

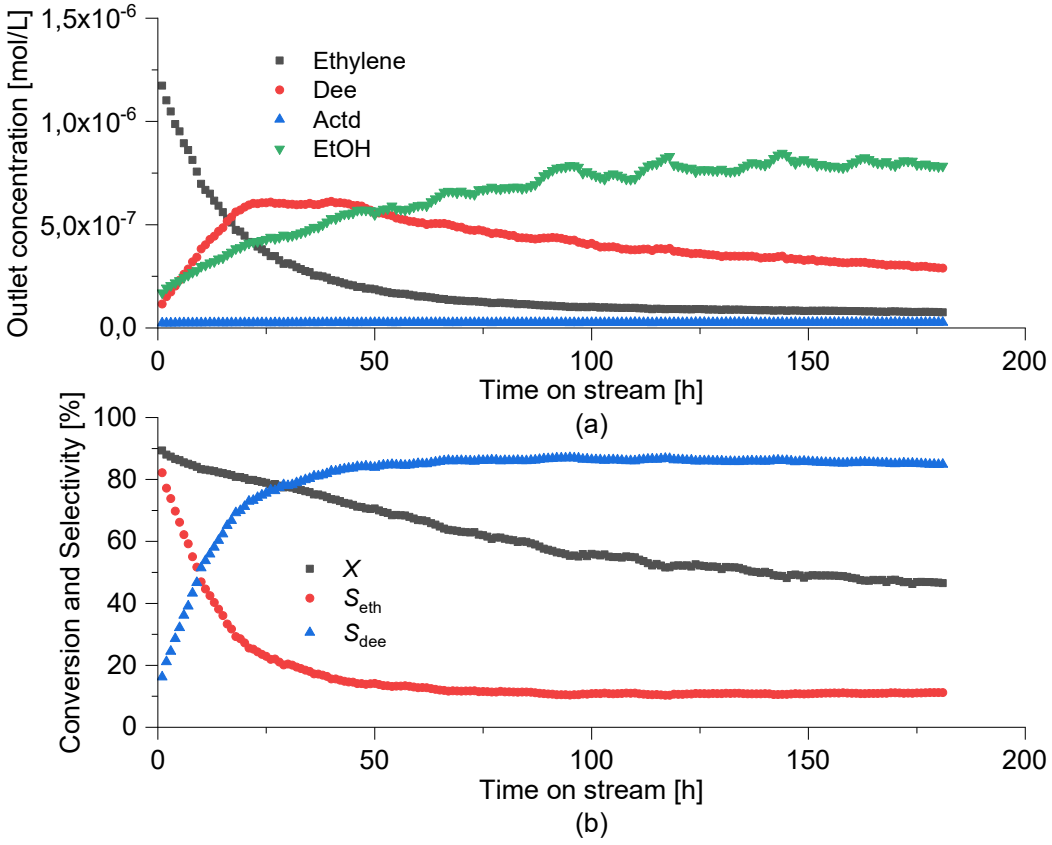

Figure 3.5. a) Product distribution and b) conversion and selectivity on time on stream over H-Beta-38 catalyst.

After the catalyst had been deactivated, the reaction was again performed in the same interval of temperatures and residences time as before, and the same procedure was followed after the catalyst regeneration. The results are presented in Figure 3.6.

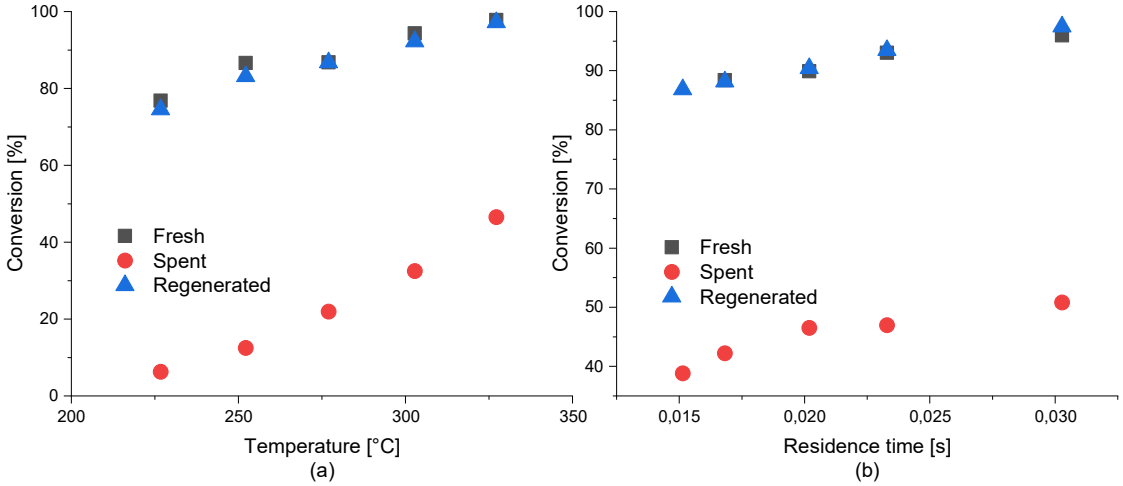

Figure 3.6. Dependence of conversion and selectivity for the fresh, spent and regenerated H-Beta-38 on a) temperature and b) residence time.

The explanation for the deactivation of H-Beta-38 during the ethanol dehydration reaction was attributed to the formation of coke (carbon deposits) on the Brønsted acid sites of the H-Beta-38 catalyst. However, the spent catalysts were possible to regenerated using synthetic air at temperature of 400 °C for duration of 240 min. The regenerated catalyst was reused in the ethanol dehydration reaction and catalytic activity was regained. The conversion of ethanol and selectivity to ethane for fresh and regenerated catalysts are almost the same (Figure 3.6). Catalytic behaviour was comparable for fresh and regenerated catalyst, indicating that H-Beta-38 was completely regenerated.

3.1.4 Sn-Beta-38

The role of tin was evaluated by exposing beta zeolite modified with tin to the same experiments as the catalysts discussed above.

Figure 3.7 groups the results of experiments performed with Sn-Beta-38. As in the previous cases, conversion and selectivities depend on both both temperature and residence time, even if such dependences are less prominent than for the proton form.

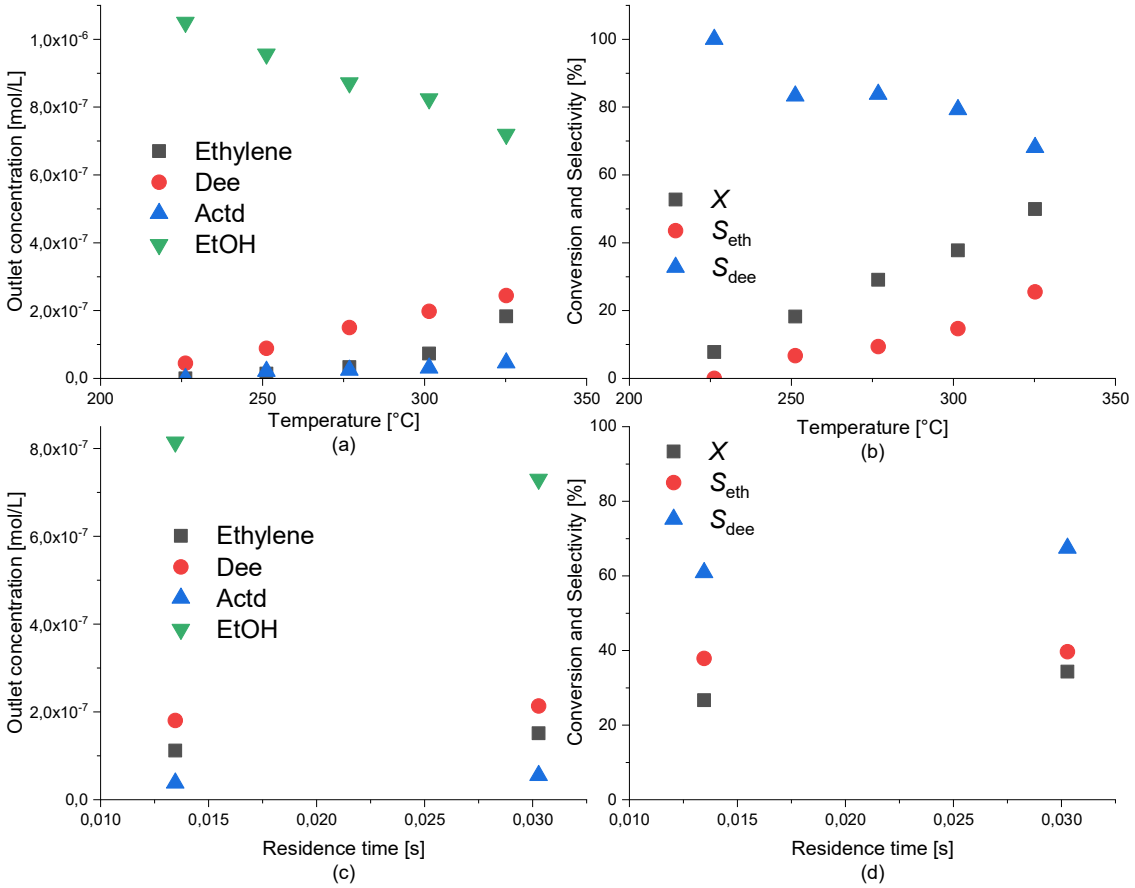

Figure 3.7. Effect of temperature and residence time on product distribution (a, c) and conversion and selectivity (b, d) over Sn-Beta-38.

Selectivity towards diethyl ether was the highest, even during deactivation. As displayed in Figure 3.8; which also shows that conversion decreased and became constant after a few hours.

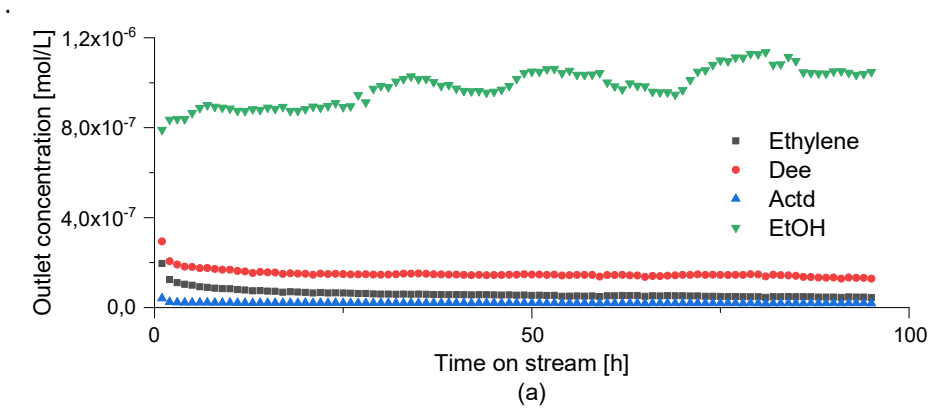

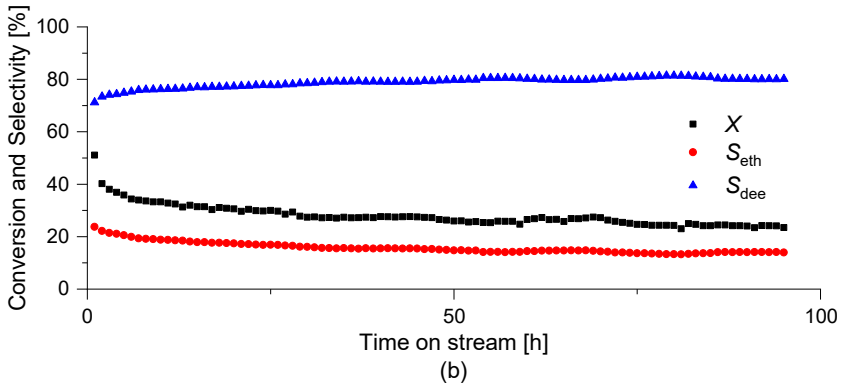

Figure 3.8. a) Product distribution and b) conversion and selectivity with time on stream for ethanol transformation over Sn-Beta-38.

Microplates coated with Sn-Beta-38 had already been tested in another reaction[5]. A possibility of catalyst regeneration was thus evaluated by runing the long term stability study secondo time.

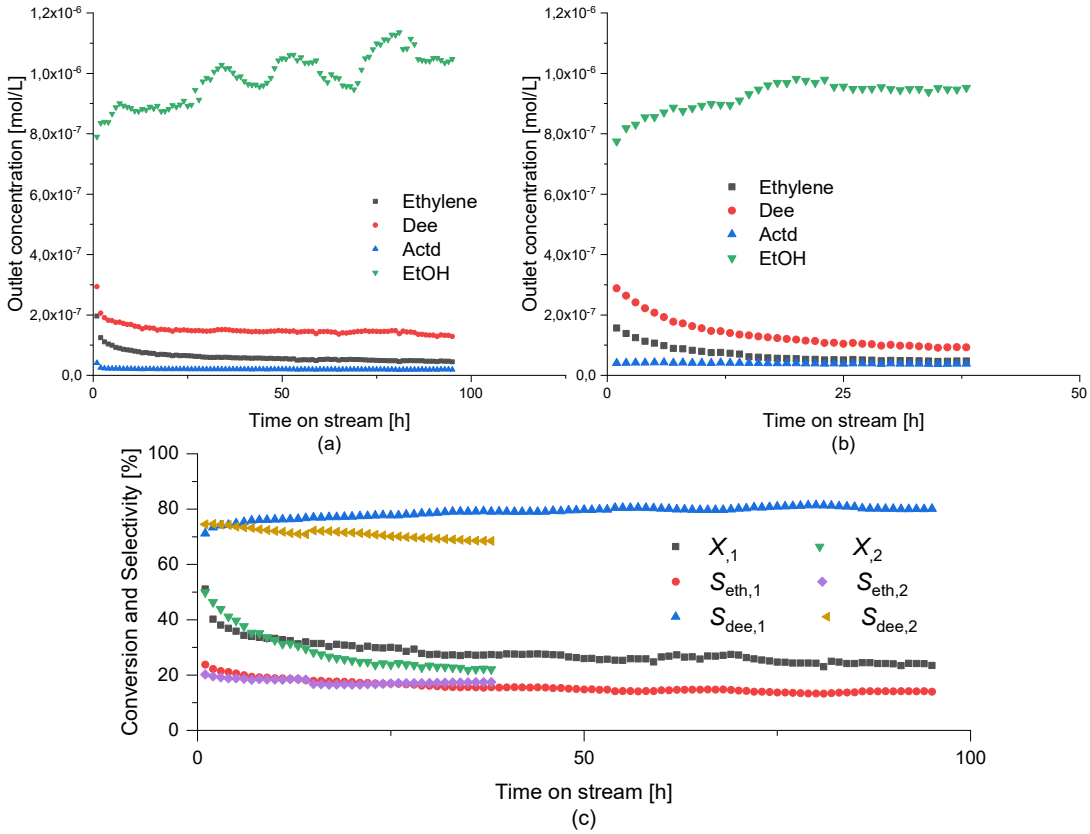

Figure 3.9. Product distribution with time on stream during the a) first and b) second durability studies with Sn-Beta-38; c) corresponding conversion and selectivities.

[5] Para-xylene formation from ethylene and 2,5-dimethylfuran.

Looking at Figure 3.9 it is possible to affirm that the deactivation was similar in both cases studied, meaning that behaviour after regeneration is comparable with the one of the fresh catalyst, even though selectivity of diethyl ether slightly diminished. Conversion during the first run had a lower value at the beginning: because of the previous experiments, it is likely that some coke was already formed, blocking some of the active sites.

The regenerated catalyst was investigated further changing temperature and residence time. While conversion up to 70% was achieved, the main product was still diethyl ether. The Sn-H-Beta-38 catalyst also exhibited deactivation with time on stream, due to coke formation on the Brønsted acid sites similar to that of H-Beta-38 catalyst. However, the deactivated Sn-H-Beta catalyst was also possible to regenerate and reuse in the ethanol dehydration reaction. Regenerated Sn-H-Beta-38 catalyst similar conversion of ethanol and selectivity to ethene as that of fresh Sn-H-Beta-38 catalyst.

3.2 Characterization

In this section results of the physico-chemical analysis are presented. Surface roughness for microplates before and after calcination is provided in §3.2.1, while §3.2.2. §3.2.3 and §3.2.5 address the crystal and pore size distributions, obtained by scanning and transmission electron microscopy. Composition of the catalysts is discussed in §3.2.4, and surface area and acidity measurements results are given in §3.2.6 and §3.2.7.

3.2.1 Surface roughness

White light confocal microscopy allows obtaining a description of the samples surface. Pristine microplates are displayed in Figure 3.10.

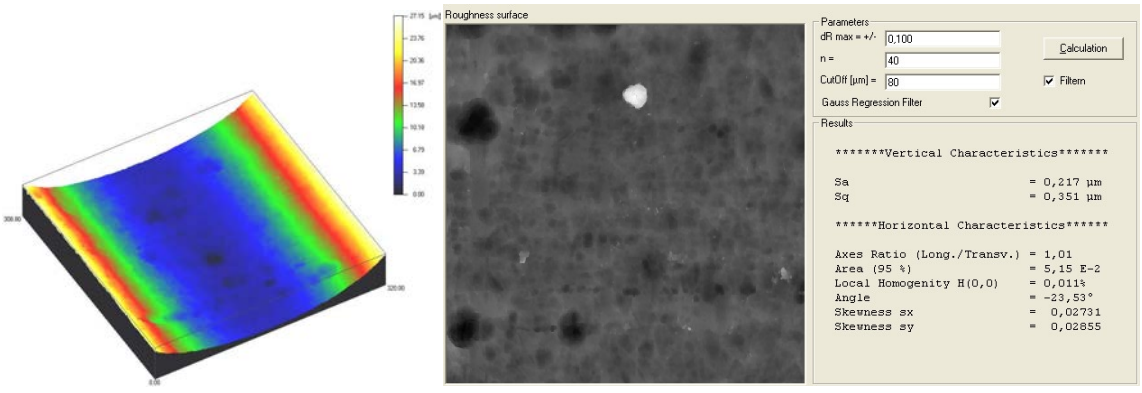

a) *b)*

Figure 3.10. a) Visualization of a microchannel of a pristine plate and b) its surface roughness obtained by white light confocal microscopy

Before calcination, the arithmetical mean height and the root mean square height were respectively 0.217 µm and 0.351 µm.

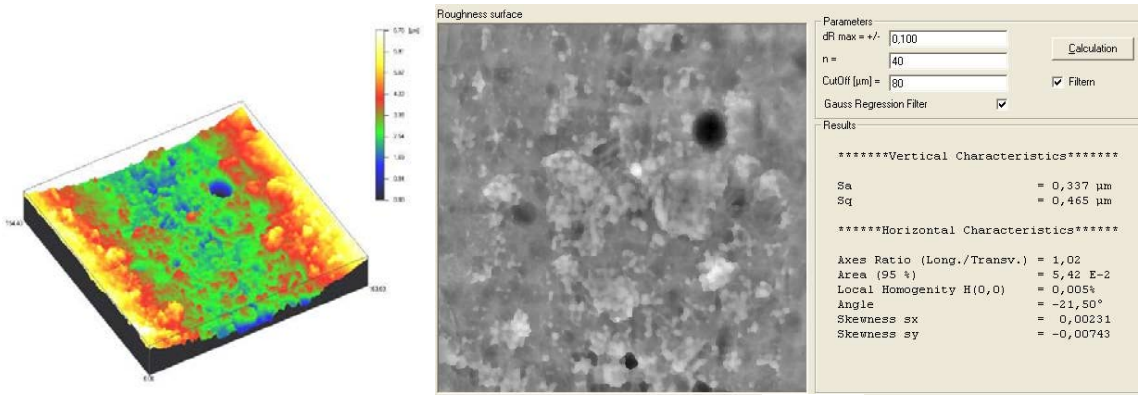

a) *b)*

Figure 3.11. a) Visualization of one microchannel of a calcined plate and b) its surface roughness obtained by white light confocal microscopy

According to Zhang (2011), calcination the microplates increases the specific surface area of the channels. For this reason, they have been increasing both the arithmetical mean height *Sa* and the root mean square height *Sq* increased, as could be observed in Figure 3.11.

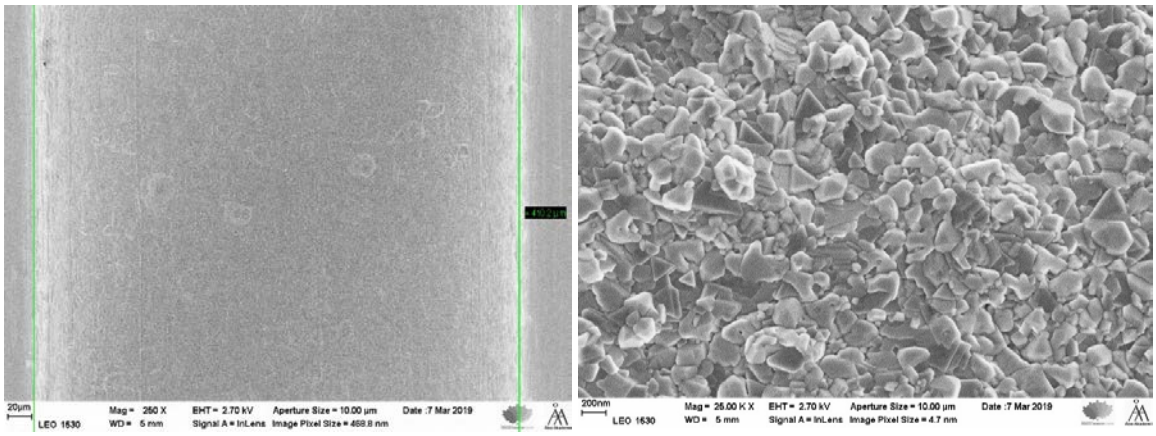

Figure 3.12. Scanning electron micrographs of a calcined plate: a) overview of the channel and b) its magnification.

SEM analysis shown in Figure 3.12 clearly illustrates and increase of the surface soughness.

3.2.2 Coating adhesion, uniformity and stability

SEM analysis was employed to visualize the adhesiveness and uniformity of the catalyst layer on the channels.

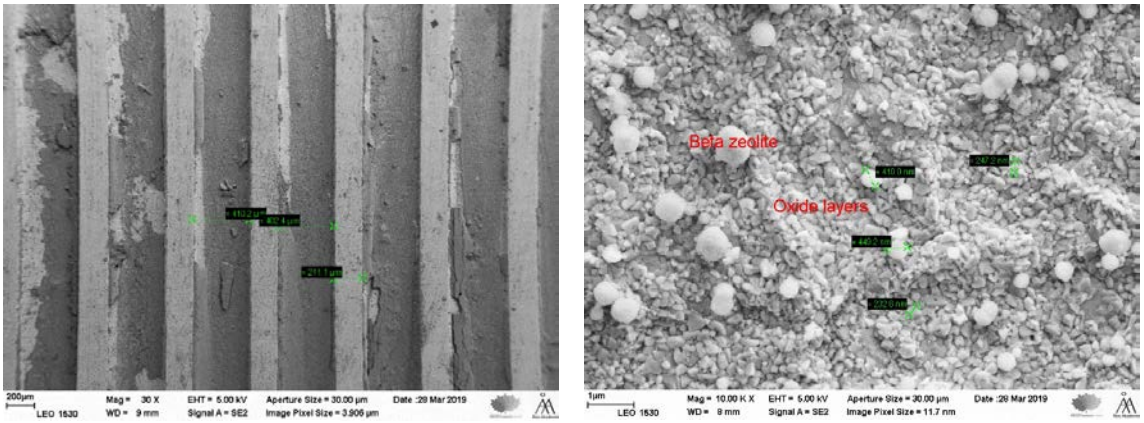

a) *b)*

Figure 3.13. Scanning electron micrographs of the first plate obtained with H-Beta-38; a) overview of the channels and b) magnification of one of the spots were the catalyst is not attached.

Figure 3.13 shows for H-Beta-38 coated plates that attachment of the catalyst layer was not uniform.

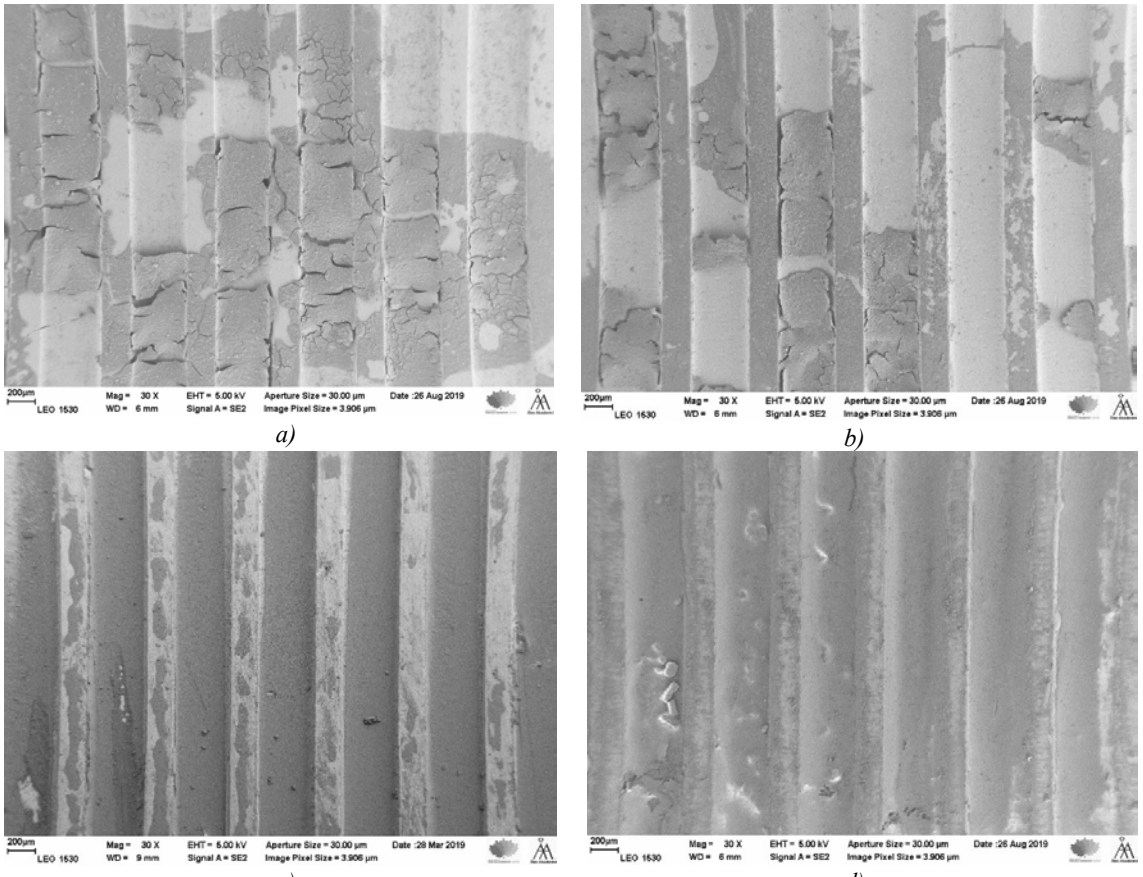

a) *b)*

c) *d)*

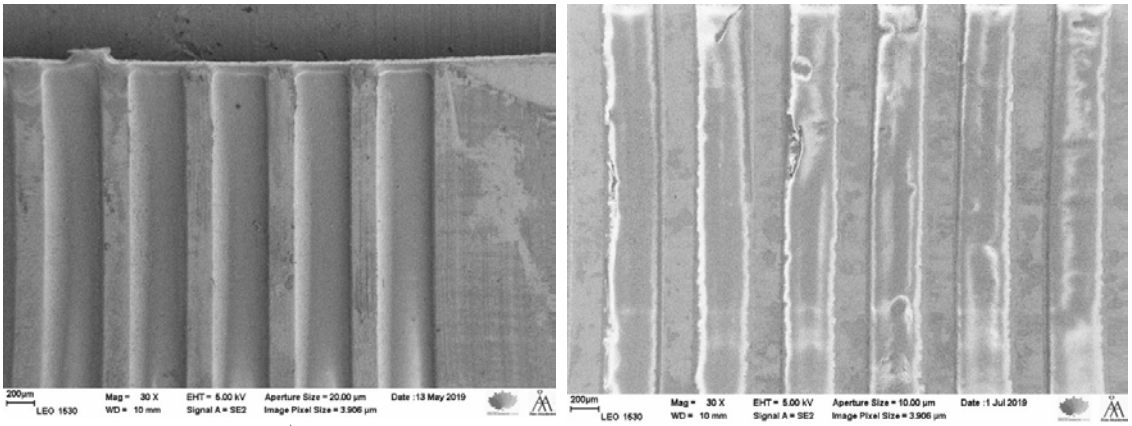

e) *f)*

Figure 3.14. Scanning electron micrographs of the plates coated with a, b) γ-alumina, c, d) H-Beta-38 and e, f) Sn-Beta-38, fresh on the left, spent on the right.

Microplates coated with the catalysts used for the reaction can be observed in Figure 3.14. What stands out is that the plates with γ-alumina (Figure 3.14.a) do not provide a good coating: the catalyst was not attach along the whole channel and there are cracks on the few spots of coating. Beta-zeolite, instead, exhibited a uniform layer: both proton and tin modified forms – Figures 3.14.c and 3.14.e respectively – proved to be good materials for coating through the slurry deposition method.

Microplates with the spent catalyst (3.14.b, d and f) did not display significant changes in the layers occurred during the reaction. Note that, in particular for Figure 3.14.f, the layers seem not to be uniform, with white spots, which can be explained by coke deposition.

3.2.3 Crystal size distribution

Finally, zooming into the coated microplates with the scanning electron microscope, it was possible to observe the particles on the catalyst layer and therefore their corresponding crystal size distribution.

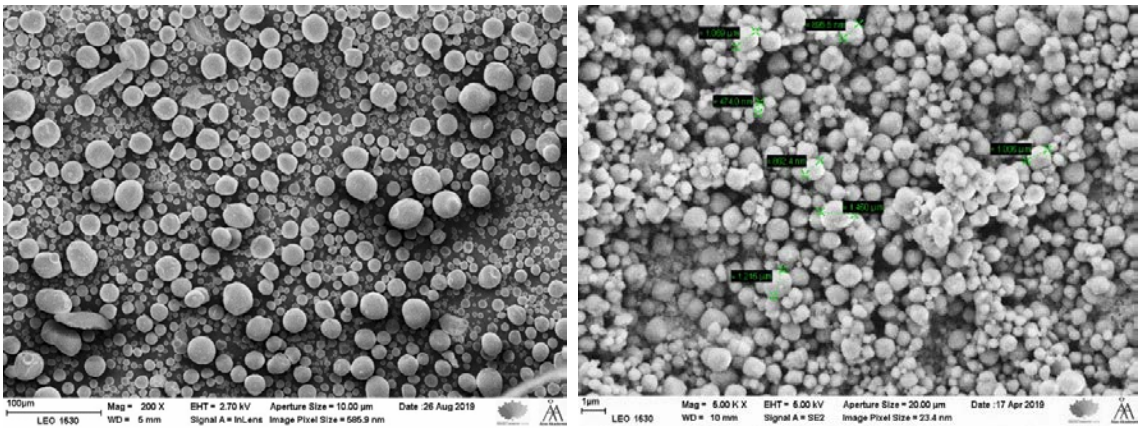

a) *b)*

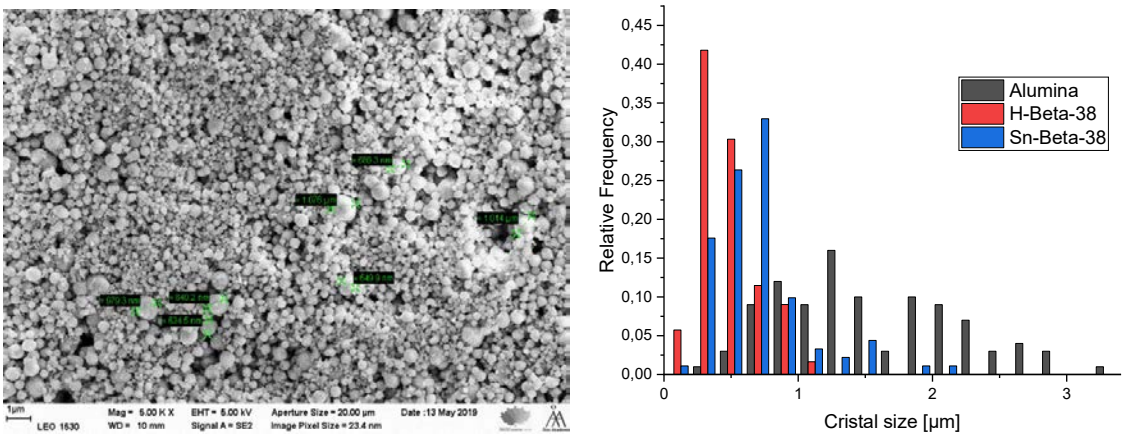

c) *d)*

Figure 3.15. Scanning electron micrographs of the plates coated with a) γ-alumina, b) H-Beta-38 and c) Sn-Beta-38 and d) their corresponding crystal size distribution.

Figure 3.15 collects micrographs for each catalyst, showing that all of them have spherical shape. From the crystal size distribution displayed in Figure 3.15.d it is possible to observe that alumina has the biggest particles and the broadest range. Note that even though particles were sieved below 32 µm for the preparation of the suspension, most of the crystals lay below 3 µm, implying that only the smallest particles were able to remain attached on the microchannel.

3.2.4 Catalyst composition

Electron dispersive X-ray analysis was used to check the value of the silica to alumina ratio provided by the manufacturer and to quantify the metal loading for Sn-Beta-38.

Table 3.1. Results of EDX for H-Beta-38 and Sn-Beta-38.

Compound	H-Beta-38	Sn-Beta-38
O [%]	66.4	66.4
Al [%]	1.7	1.7
Si [%]	31.9	29.3
Sn [%]	0	2.6
Al_2O_3 [%]	4.3	3.9
SiO_2 [%]	95.7	78.7
SnO_2 [%]	0	17.4
SiO_2/Al_2O_3 [-]	22	20

Table 3.1 shows the results of this analysis. It can be easily noticed that the silica to alumina ratio of H-Beta-38 is lower than the one provided by the supplier, meaning that the catalyst is more acid than anticipated.

The presence of tin in the modified form of the beta zeolite confirms that the metal was successfully introduced. SiO_2/Al_2O_3 decreased after introduction of tin.

3.2.5 Pore size distribution

The powder form of the catalysts was analysed by transmission electron microscopy to access at the pore distribution and size. Results are displayed in Figure 3.16.

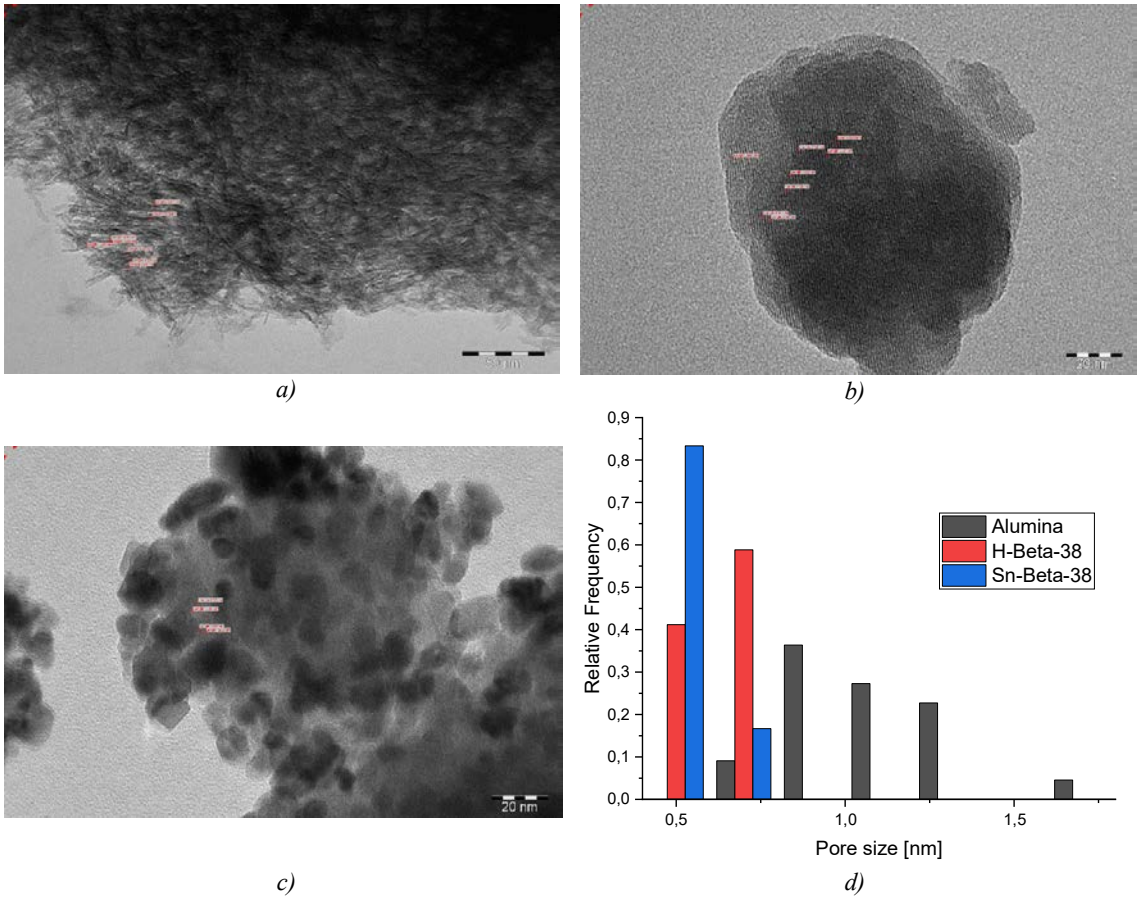

Figure 3.16. Transmission electron micrographs of a) γ-alumina, b) H-Beta-38 and c) Sn-Beta-38 and d) their corresponding pore size distribution.

Figure 3.16.b, displaying one particle of H-Beta-38, illustrates that the pore distribution is very uniform with straight channels. The same structure was maintained after the metal modification (Figure 3.16.c) and it is possible to observe rather uniform distribution of tin on the particles. Alumina, instead, exhibits a completely different structure, with tortuous and larger pores, as can be confirmed from the pore size distribution in Figure 3.16.d. Pore dimensions of the beta zeolite lay in a narrower range in comparison with γ-alumina.

3.2.6 Surface area

Nitrogen physisorption allowed the evaluation of the specific surface area and the pore volume of the three catalysts. The results are presented in Table 3.2.

Table 3.2. Values of specific surface area and micropore volume obtained with performing N_2 physisorption on the catalysts.

	γ-alumina	**H-Beta-38**	**Sn-Beta-38**
Specific surface area [m^2/g]	267	827	532
Micropore volume [cm^3/g]	0	0.3	0.2

Looking at the values displayed in Table 3.2, it is possible to observe that H-Beta-38 is the catalyst with the highest specific surface area, three-fold higher than for alumina. A lower surface area of the tin modified beta is probably due to the presence of metal clusters, which can block some of the pores.

3.2.7 Acidity

Finally, the results of FTIR measurements for the amount of Brønsted and Lewis acid sites are shown in Table 3.3.

Alumina has the lowest concentration of acid sites, which are mostly Lewis ones. Beta zeolites, instead, have higher concentrations of Brønsted acid sites, and the deposition of metal promoted the formation of some Lewis acid sites, at the expense of some of Brønsted ones.

Table 3.3. Acid sites concentration of γ-alumina, H-Beta-38 and Sn-Beta-38 obtained by FTIR.

	Concentration [µmol/g]					
	γ-alumina		**H-Beta-38**		**Sn-Beta-38**	
	BAS	LAS	BAS	LAS	BAS	LAS
Weak	1	24	17	19	0	29
Medium	1	4	40	9	133	4
Strong	0	1	221	2	70	2
Sum	**3**	**29**	**278**	**31**	**203**	**36**

The concentration of acid sites changed during catalyst deactivation and it would be very intresting to perform FTIR on the spent catalysts. This was not possible, however, because the catalyst is attached to the microplates and, even if scratched, the amount would not be sufficient for the analysis.

3.3 Discussion

Dehydration of ethanol to ethylene is an endothermic reaction: an increase of temperature, therefore, provides an increase of the production of ethylene, as demonstrated by the product distribution for the thermal reaction (Figure 3.1.a). This reaction is promoted by the presence of acid sites, namely Brønsted and Lewis ones, which however affect differently the reaction pathways. When catalysed by γ-alumina, mainly diethyl ether was produced, while H-Beta-38 promoted the formation of ethylene. From Table 3.3 the difference between these two catalysts is related to a much higher concentration of Brønsted sites in the latter. Further confirmation is obtained by the experiments performed with Sn-Beta-38: some of the Brønsted sites were substituted by the metal modification of H-Beta-38, promoting formation of Lewis ones, that in turn was beneficial for the formation of diethyl ether. Acetaldehyde formation can be also related to the catalysis by iron, present in stainless steel from which microplates are manufactured.

From the catalyst durability studies, it is possible to observe that the Lewis acid sites do not undergo to deactivation since both conversion and selectivity were constant for long run experiments. Zeolite catalysts, instead, deactivated. During deactivation of H-Beta-38 selectivity changed, becoming higher for diethyl ether. This means that Brønsted acid sites deactivated while taking into consideration the results obtained with alumina, it is likely that Lewis ones did not.

From the reaction point of view, H-Beta-38 can be therefore selected as a promising catalyst. The proton form of this zeolite is the one with the highest surface area, with the narrowest crystal size distribution on microplates and pore size distribution. Moreover, this material allowed to obtain a very good coating. Using the slurry deposition method, the catalyst was attached on the channels, distributing very uniformly. The drawback of this catalyst is mainly related to its deactivation, which inhibits the formation of ethylene.

These considerations have been taken into account for development of the kinetic model of the reaction, which is described in Chapter 4.

The Lewis acid sites, which are the most abundant in γ-alumina, are stable over time and promote formation of diethyl ether.

Brønsted acid sites of the beta zeolite resulted in formation of ethylene, being however prone to deactivation. Lewis acid sites in beta zeolites, which do not deactivate according to the studies performed with γ-alumina, foster production of diethyl ether.

Chapter 4

Kinetics

Description of kinetics has been developed for the reaction catalysed by H-Beta-38 since this catalyst turned out to be the best one in terms of ethylene production. The reaction mechanism for ethylene and diethyl ether formation takes into account ethylene generation on Brønsted acid sites, which deactivate, while diethyl ether on Lewis ones, which are stable. Reaction mechanism of acetaldehyde generation was not investigated, because of the low amounts produced; but its formation was considered in kinetic modelling.

4.1 Reaction mechanism

The reaction mechanism has been assessed according to the results obtained in the microreactor. As discussed in §3.3 and illustrated in Figure 4.1, ethylene is assumed to be formed on the Brønsted acid sites, while diethyl ether is mainly produced on Lewis ones.

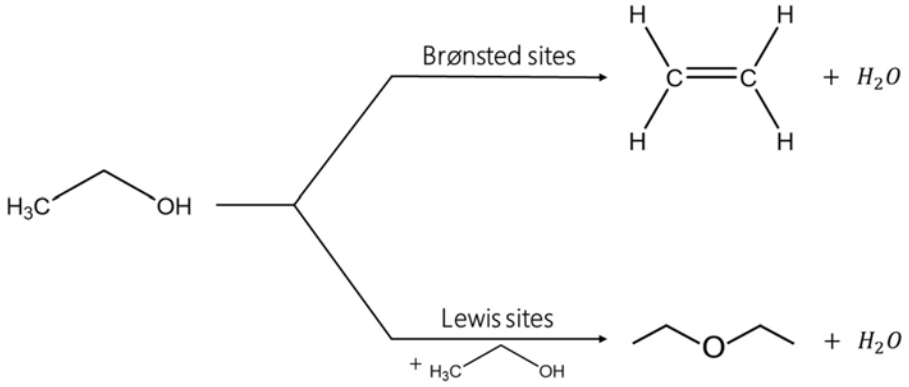

Figure 4.1. Reaction network of ethanol dehydration over H-Beta-38.

Production of acetaldehyde was included in the mass balance, as explained in §4.2.
The elementary steps in the reaction mechanism are reported in Equation (4.1) to (4.6).

$$C_2H_5OH + B^* \equiv C_2H_5OHB^* \quad (4.1)$$

$$C_2H_5OHB^* \rightarrow C_2H_4B^* + H_2O \quad (4.2)$$

$$C_2H_4B^* \equiv C_2H_4 + B^* \quad (4.3)$$

$$C_2H_5OH + L^* \equiv C_2H_5OHL^* \quad (4.4)$$

$$2C_2H_5OHL^* \rightarrow (C_2H_5)_2O\ 2L^* + H_2O \quad (4.5)$$

$$(C_2H_5)_2O\ 2L^* \equiv (C_2H_5)_2O + 2L^* \quad (4.6)$$

Equations (4.1), (4.3), (4.4) and (4.6) represent steps of quasi-equilibrium: adsorption is assumed to be fast and to lead quickly to equilibrium. Equations (4.2) and (4.5) represent instead the actual reaction from ethanol to ethylene and diethyl ether, respectively. These steps are assumed to be irreversible: residence time in the microreactor is so small that is unlikely to think about reverse reactions.

4.2 Kinetic modelling

The model describing the reaction takes into account deactivation of the catalyst since it is not negligible; the following hypotheses have been used:

1. Brønsted acid sites deactivate exponentially with time, as displayed in Equation (4.7); the kinetic constant of deactivation needs to be retrieved;

$$c_B(t) = c_B^0 \cdot e^{-k_d \cdot t} \quad (4.7)$$

2. Lewis acid sites do not deactivate, so their concentration is constant and equal to the one obtained by FTIR results listed in §3.2.7 – Equation (4.8)

$$c_L(t) = c_L^0 \quad (4.8)$$

3. Adsorption and desorption do not change, so their kinetic constants are constant;

4. Adsorption is considered to be reversible, allowing to use partial equilibrium approximation. Its kinetic constant can, therefore, be calculated as the ratio between adsorption and desorption kinetic constants. Equations (4.9) – (4.12) show their expressions;

$$K_1 = \frac{c_{C_2H_5OHB^*}}{c_{C_2H_5OH} \cdot c_{B^*}} \quad (4.9)$$

$$K_3 = \frac{c_{C_2H_4} \cdot c_{B^*}}{c_{C_2H_4B^*}} \tag{4.10}$$

$$K_4 = \left(\frac{c_{C_2H_5OHL^*}}{c_{C_2H_5OH} \cdot c_{L^*}} \right)^2 \tag{4.11}$$

$$K_6 = \frac{c_{(C_2H_5)_2O} \cdot c_{L^*}^2}{c_{(C_2H_5)_2O\,2L^*}} \tag{4.12}$$

K_4 presents squares of the concentrations because Equation (4.4) needs to be multiplied by two in order to match stoichiometry of the following steps leading to diethyl ether.

5. Steps of the reaction identified by Equations (4.2) and (4.5) follow the Arrhenius law:

The reaction rates of ethylene and diethyl ether formation, which represent the rate determining steps, are displayed by Equations (4.13) and (4.14).

$$r_{C_2H_4} = k_2 \cdot c_{C_2H_5OHB^*} \tag{4.13}$$

$$r_{C_2H_4} = 2 \cdot k_5 \cdot \left(c_{C_2H_5OHL^*}\right)^2 \tag{4.14}$$

Making explicit the expression for the concentration of adsorbed ethanol from Equations (4.9) and (4.11), Equations (4.13) and (4.14) can be written as in (4.15) and (4.16)

$$r_{C_2H_4} = k_2 \cdot K_1 \cdot c_{C_2H_5OH} \cdot c_{B^*} \tag{4.15}$$

$$r_{C_2H_4} = 2 \cdot k_5 \cdot K_4 \cdot \left(c_{C_2H_5OH} \cdot c_{L^*}\right)^2 \tag{4.16}$$

Concentration of Brønsted and Lewis acid sites can be written as function of the total balance of active sites – Equations (4.17) and (4.18).

$$c_B(t) = c_{B^*} + c_{C_2H_5OHB^*} + c_{C_2H_4B^*} \tag{4.17}$$

$$c_L(t) = c_{L^*} + c_{C_2H_5OHL^*} + c_{(C_2H_5)_2O\,2L^*} \tag{4.18}$$

Substituting values of adsorbed species from Equations (4.9) – (4.12) and writing the explicit equations for concentration of Brønsted and Lewis acid sites are obtained:

$$c_{\mathrm{B}^*} = \frac{c_{\mathrm{B}}(t)}{1 + K_1 c_{\mathrm{C_2H_5OH}} + K_3^{-1} c_{\mathrm{C_2H_4}}} \tag{4.19}$$

$$c_{\mathrm{L}^*} = \frac{c_L(t)}{1 + K_4^{1/2} \cdot c_{\mathrm{C_2H_5OH}} + K_6^{-1} c_{\mathrm{C_2H_5OH}} \cdot c_{\mathrm{L}^*}} \tag{4.20}$$

The final reaction rates were obtained substituting Equations (4.19) and (4.20) in Equations (4.15) and (4.16):

$$r_{C_2H_4} = \frac{k_1' \cdot c_{\mathrm{C_2H_5OH}}}{D_1} \cdot c_B(t) \tag{4.21}$$

$$r_{(C_2H_5)_2O} = \frac{k_2' \cdot \left(c_{\mathrm{C_2H_5OH}}\right)^2}{(D_2)^2} \cdot (c_L^0)^2 \tag{4.22}$$

where kinetic constants are lumped (K_1 and k_2; k_4 and K_5) and denominators D_1 and D_2 are the ones displayed in Equations (4.19) and (4.20). Moreover, the concentration of Lewis sites is not time-dependent since it is assumed to be constant.

The Reynolds number has been roughly estimated, calculating the hydraulic diameter of the channels and using helium as reference gas for the calculation of viscosity (ca. 95 % v/v is occupied by the inert gas). At the different temperatures and volume flows exploited, Re lays between 4 and 10, so the flow in microreactor is laminar.

4.3 Reactor model

Reaction rates are then used for solving the mass balances. Microreactors can be assumed to behave like plug flow reactors, where the mass transfer is not limiting, thus the reaction is under kinetic control. The corresponding mass balance is:

$$\varepsilon \frac{\mathrm{d}c}{\mathrm{d}t} = -\frac{\mathrm{d}\dot{n}_{\mathrm{i}}}{\mathrm{dV}} + r_{\mathrm{i}} \cdot \rho_{\mathrm{cat}} \tag{4.23}$$

Assuming the gas volume fraction ε equal to 1, because of the thin catalyst layer, and pseudo-steady state, Equation (4.24) can be obtained:

$$\frac{\mathrm{d}\dot{\mathrm{n}}_{\mathrm{i}}}{\mathrm{dV}} = r_{\mathrm{i}} \cdot \rho_{\mathrm{cat}} \tag{4.24}$$

Dividing by the reactor volume, the final model is obtained:

$$\frac{\mathrm{d}\dot{\mathrm{n}}_{\mathrm{i}}}{\mathrm{d}t} = r_{\mathrm{i}} \cdot \mathrm{m}_{\mathrm{cat}} \tag{4.25}$$

However, the exact amount of catalyst attached on the microplates is not known. For the sake of simplicity, therefore, PFR has been substituted by a series of tank reactors (Schmidt, L. D., 2005): 50 CSTRs have been used. The corresponding mass balance is calculated considering inlet, outlet, production and consumption terms, as given by Equation (4.26). Using Equations (4.27) and (4.28) it can be written as a function of concentrations – Equation (4.29), to compare calculations obtained with the GC analysis.

$$\begin{cases} \dot{n}_i^{in} + r_i \cdot V_R = \dot{n}_i^{out} + \dfrac{\partial n_i}{\partial t} & (4.26) \\ \dot{n}_i = c_i \cdot \dot{V}_{tot} & (4.27) \\ n_i = c_i \cdot V_R & (4.28) \end{cases}$$

$$V_R \frac{\partial c_i}{\partial t} = \left(c_i^{in} - c_i^{out}\right) \cdot \dot{V}_{tot} + r_i \cdot V_R \tag{4.29}$$

Calculating the residence time as in Equation (4.30) and substituting it in (4.29), it is possible to obtain the final mass balance.

$$\tau = \frac{V_R}{\dot{V}_{tot}} \tag{4.30}$$

$$\frac{\partial c_i}{\partial t} = \frac{c_i^{in} - c_i^{out}}{\tau} + r_i \tag{4.31}$$

The material balance in Equation (4.31) was implemented in the kinetic modelling parameter estimation, where unknown parameters were determined by minimizing the difference between calculations and experiments. Equation (4.31) is solved for ethylene and diethyl ether using the reaction rates defined by Equations (4.21) and (4.22) respectively. The same material balance has been used for acetaldehyde production. A fourth reaction was also considered, where ethylene reacted an unknown product. Reaction rates of these two secondary reactions have

been assumed to follow the Arrhenius law. The inlet concentration of ethylene was calculated as well because of its variations.

Deactivation has been taken into account not only for the catalyst durability studies, but for all experiments. The reaction has been tested at different temperatures and residence times, and three experimental points have been taken for each operating condition[6] – results collected in Chapter 3 represent the mean of these data. For the kinetic modelling, on the contrary, each data point has been considered in the evaluation of deactivation from the very beginning.

Software ModEst was used, minimizing the discrepancy between experiments and calculations with the Levenberg method. The results are displayed in Figures 4.2, 4.3 and 4.4.

Figure 4.2 displays the experimental data and the calculations, illustrating that the kinetic model, despite its simplicity, is able to describe the influence of temperature and residence time on catalytic behaviour, capturing also catalyst deactivation.

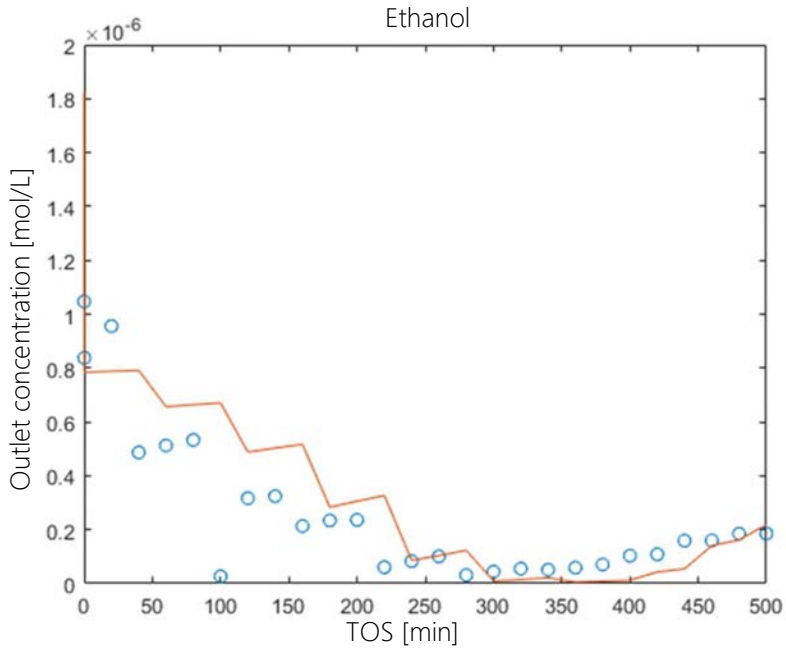

Figure 4.2. Model and experimental data profile of outlet concentration of ethanol.

[6] Each experiment has been run at the same conditions for ca. one hour, in order to have enough time for three GC analyses.

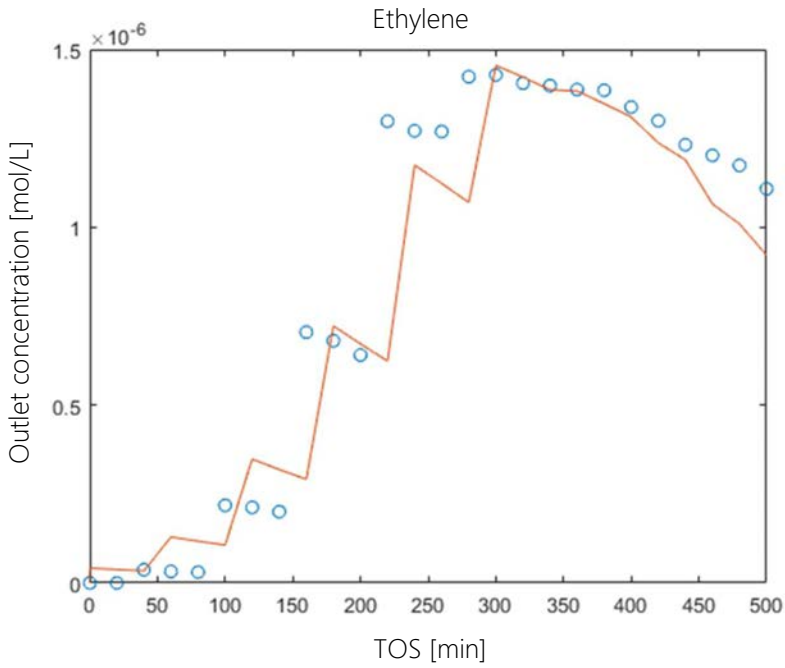

Figure 4.3. Model and experimental data profile of outlet concentration of ethylene.

In Figure 4.3 the same plot is presented for ethylene formation. The reaction rate given in Equation (4.21) seems to be able to follow the pathway obtained with the experiments, confirming that the mechanism figured is the one taking place in the reactor.

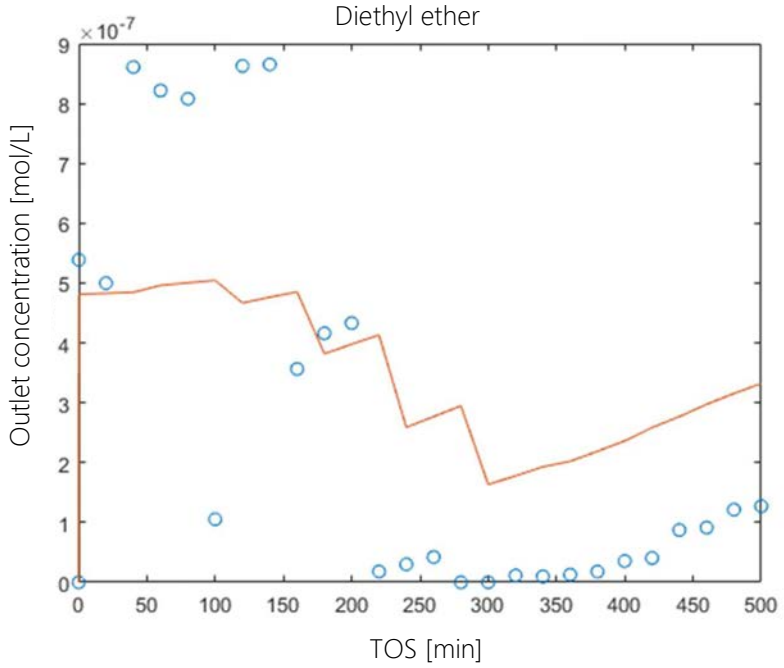

Figure 4.4. Model and experimental data profile of outlet concentration of diethyl ether.

Finally, the outlet concentration of diethyl ether is displayed in Figure 4.4. Fitting seems to capture at least the trend: diethyl ether production is higher at the beginning and diminishing with an increase of temperature. It starts to increase again when Brønsted acid sites are blocked.

Calculated parameters are listed in Table 4.1.

Table 4.1. Values of pre exponential factors A and activation energies Ea [kJ/mol] obtained by fitting.

	A	**Ea**
Ethylene	6.28 ± 9.13	128·± 32
Diethyl ether	$1.71 \cdot 10^{7} \pm 0$	20 ± 5
Acetaldehyde	2.27 ± 18.2	56.8 ± 273
Unknown products	$1.49 \cdot 10^{-1} \pm 130$	$27.9 \pm (1.97 \cdot 10^{4})$

Pre exponential factors[7] and activation energies of each reaction involved have been obtained. The activation energy of ethylene formation is the highest one, confirming experimental observations. Pre exponential factor of diethyl ether formation is very high, and this may be related to the fact that there is the need for two molecules of ethanol for producing it.
Relative errors of *A* and *Ea* for the reactions for acetaldehyde and unknown products formation are very high, which is related to their low concentrations.

Two more parameters have been obtained in the simulations:

- $c^{\mathrm{in}}_{\mathrm{C_2H_5OH}} = (1.82 \pm 0.2)\ 10^{-6}$ mol/L
- $k_{\mathrm{d}} = (5.08 \pm 0.9)\ 10^{-3}$ 1/min

The inlet concentration of ethanol is quite similar to the one calculated during the experiments ($1.11 \cdot 10^{-6}$ mol/L), which is the mean of different values. The calculated value can be therefore closer to the actual amount of ethanol flowing into the reactor during experiments with H-Beta-38.
The value of the deactivation constant is quite small, in agreement with the fact that complete catalyst deactivation required several days.

[7] Unit of measure of the pre exponential factors change from different reactions, according to their order.

Conclusions

In this work, a study on the dehydration of ethanol was carried out in a microreactor, using solid acidic catalysts. The objective of this study was to understand how catalysts influence the production of ethylene, and to understand the reaction kinetics.

Ethanol dehydration represents a way of obtaining ethylene from biomass. Oil supplies diminished significantly in the last decades, and they are not going to last forever: for this reason, there is an interest in producing commodities from different sources. Ethanol dehydration may lead mainly to ethylene, diethyl ether and acetaldehyde: the scope of this work was to understand the conditions that enhance the production of ethylene.

A gas phase microreactor was used during these experiments, provided by the Institute für Mikrotechnik Mainz GmbH (IMM). The reaction section consists of ten microplates, each of them having nine microchannels, where the reactant flows in. Microplates have been calcined to increase their surface area, and thereafter coated with the catalyst by a slurry deposition method from an ammonia containing suspension. Slow drying was achieved placing the coated plates in the fridge.

Pristine and coated microplates, and the powder forms were analysed by several physico-chemical methods. Platelets were analysed with white light confocal microscopy before and after the step calcination to perceive its influence on the surface roughness. Once coated, microplates were placed in an ultrasound bath, to assess the adhesion of the catalyst layer. Further analysis was performed with SEM. For better understanding the catalytic behaviour on the reaction, powder forms of γ-alumina, H-Beta-38 and Sn-Beta-38 were analysed with SEM-EDX, TEM, FTIR and nitrogen physisorption; these methods were used to determine, respectively, the silica to alumina ratio, distribution of porosity, concentration of acid sites Sn nanoparticles size, crystal size of Beta zeolites and the specific surface area and pore volume. Beta zeolites resulted in a very good uniform coating, well distributed along the whole surface of the microchannels, while γ-alumina coated plates had weak adhesion and their crystal size distribution had a broader range than the two other catalysts. H-Beta-38 was the most acidic catalyst, bearing mostly Brønsted acid sites, having the highest surface area. Tin deposition on beta zeolite led to a decrease of some Brønsted sites and an increase of Lewis one. Application of the metal clusters blocked some pores, decreasing the surface area. According to EDX, the silica to alumina ratio was 22 indicating that the material was more acidic than anticipated.

The reaction was run at first without a catalyst, then with coated plates. For the uncatalysed reaction, 400 °C was necessary to obtain meaningful values of conversion and selectivity. γ-alumina and Sn-Beta-38 promoted mainly formation of diethyl ether, demonstrating that diethyl ether is mainly produced on Lewis acid sites, while a small amount of acetaldehyde may be due to stainless steel composing the microplates. A high concentration of Brønsted acid sites in H-Beta-38, instead, enhanced formation of ethylene. Conversion was almost complete at 325 °C, with ethylene selectivity reaching 98 %. Although initially selectivity was very high, these Brønsted active sites deactivated with time on stream, and after ca. 20 hours diethyl ether became the most abundant product. The same catalyst durability studies were performed on two other two catalysts, showing that while Sn-Beta-38 had a higher deactivation rate than the proton form, γ-alumina was stable.

It could be speculated from these results that Brønsted acid sites deactivate, while Lewis ones, i.e. the only ones present on γ-alumina, did not. Confirmation of this hypothesis could be obtained, for example, by analysing the spent catalyst with FTIR, which is however very challenging.

This represents one of the main limitations of microreactors: post-run analysis is extremely difficult, because the amount of catalyst scratched from the microplates could be not sufficient for performing analysis. Moreover, calculation of the exact catalyst amount deposited is far from being straightforward. On top of this, flow rates are very small, which means that small changes in the set-up affect significantly the values of calculated concentrations. In this particular case, an inlet concentration of ethanol is both effected by fluctuations in the helium flow and in the temperature of the thermostat.

For H-Beta-38, displaying the best performance in terms of ethylene production, the reaction kinetics has been exploited. Formation of ethylene was related to the amount of Brønsted acid sites, which decrease exponentially with time on stream during the reaction because of deactivation.
Diethyl ether production, instead, is related to concentration of Lewis acid sites, which do not deactivate, as demonstrated by the results obtained with γ-alumina. The reaction network included formation of ethylene, diethyl ether and acetaldehyde.

The proposed kinetic model was able to fit properly the outlet concentrations of both ethanol and ethylene. In particular the model was able to describe the influence of temperature and residence time on the reaction taking into consideration also deactivation of the Brønsted acid sites. The fitting was not as accurate for diethyl ether, being however an order of magnitude smaller. Nevertheless, the description can still be considered acceptable.

Future studies may be related to the elucidation of the effect of temperature on deactivation of H-Beta-38, aiming at finding conditions allowing the best compromise between ethylene production and deactivation. Moreover, comparison of microreactors with conventional reactors, including economic analysis, should be performed.

Notation

A	=	pre exponential factor
A^{GC}	=	area obtained from the GC results [pA s]
c	=	concentration [mol/L]
Ea	=	activation energy [J/mol]
K	=	adsorption-desorption equilibrium constant [-]
k	=	kinetic constant
MW	=	Molecular weight [g/mol]
$\dot{n}$	=	molar flow [mol/min]
P	=	operative pressure [Pa]
r	=	reaction rate [mol/L s]
R	=	ideal gas constant [J/mol K]
Re	=	Reynolds number [-]
RF	=	reference factor [mol/L pA s]
t	=	time [s]
T	=	operative temperature [K]
$\dot{V}$	=	volume flow [mL/min]
V_{R}	=	reactor volume [mL]
X	=	conversion [-]
S	=	selectivity [-]

Greek letters

ε	=	gas volume fraction [-]
ρ	=	density
ν	=	stoichiometric coefficient [-]
τ	=	residence time [s]

Acronyms

EDX	=	electron dispersive X-ray analysis
FTIR	=	Fourier transform infrared spectroscopy
GC	=	gas chromatography/chromatographer
SEM	=	scanning electron microscopy
TEM	=	transmission electron microscopy
TOS	=	time on stream [min]

Appendix

A.1.Reaction set-up

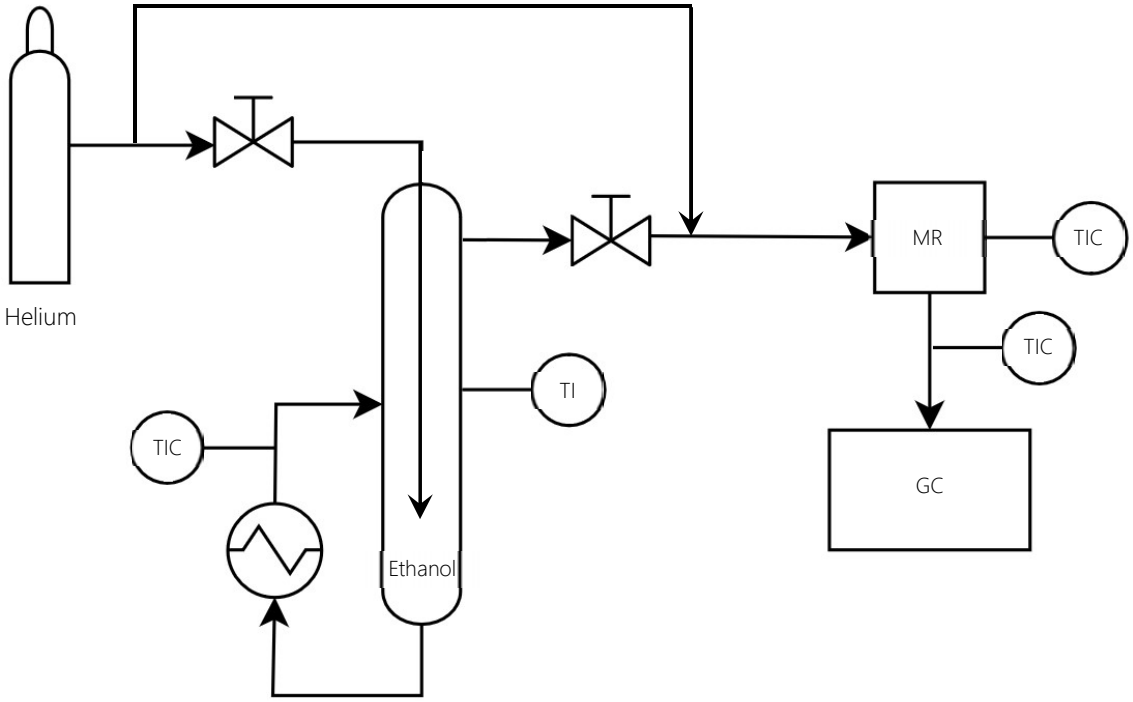

Figure A.1. Schematic representation of the reaction system.

A.2. Mass balance

Calculating the inlet concentration of ethanol from the outlet products, it is necessary to check the mass balance corresponding to the constant inlet concentration assumed, as indicated in Equation (A.1). This allows considering also the

$$\text{MB [\%]} = \frac{\sum(c_{\text{i}}^{\text{out}} \cdot \text{MW}_{\text{i}})}{\text{c}_{\text{C}_2\text{H}_5\text{OH}}^{\text{in}} \cdot \text{MW}_{\text{C}_2\text{H}_5\text{OH}}} \cdot 100 \tag{A.1}$$

Fluctuations that can be observed in Figures A.1-A.5 can be mainly correlated to the fluctuations in the actual inlet concentration of ethanol.

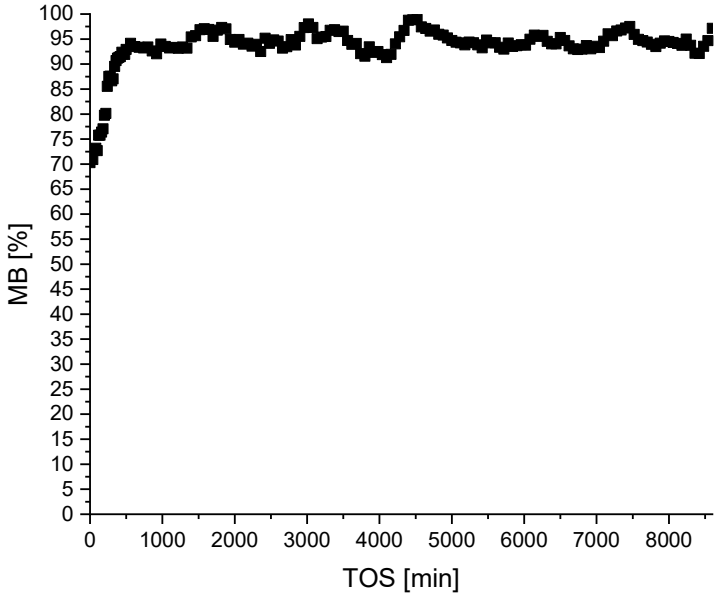

Figure A.2. Mass balance with time on stream over γ-alumina.

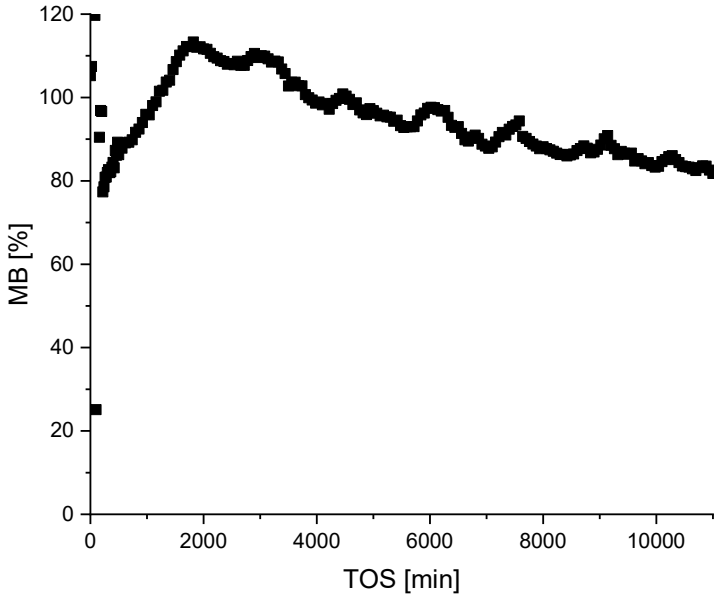

Figure A.3. Mass balance with time on stream over fresh H-Beta-38.

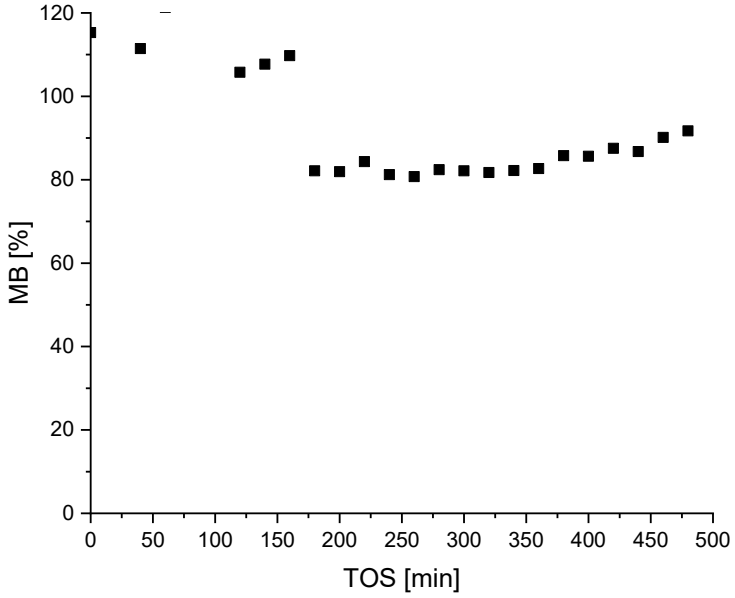

Figure A.4. Mass balance with time on stream over regenerated H-Beta-38.

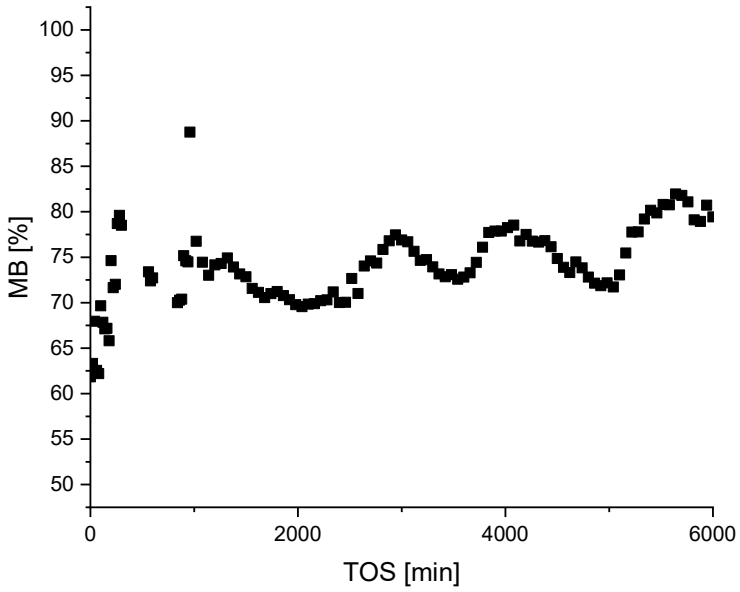

Figure A.5. Mass balance with time on stream over fresh Sn-Beta-38.

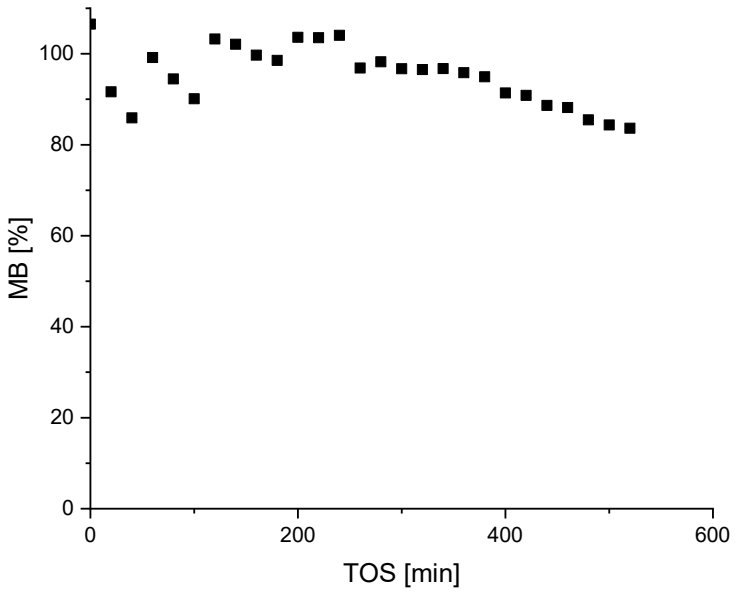

Figure A.6. Mass balance with time on stream over regenerated Sn-Beta-38.

References

Ehrfeld, W., V. Hessel and H. Löwe (2000). State of the Art of Microreactor Technology in *Microreactors. New Technology for Modern Chemistry* (1st ed.). Wiley-VCH, Weinheim (Federal Republic of Germany).

Egerton, R. F. (2005). The scanning electron microscope. In: *Physical principles of electron microscopy: an introduction to TEM, SEM, and AEM*. Springer, 202.

Eggersdorfer, M., J. Meyer and P. Eckes (1992). Use of renewable resources for non-food materials. *FEMS Microbiol. Rev.*, **103**, 355-364.

Emeis, C. A. (1993). Determination of Integrated Molar Extinction Coefficients for Infrared Absorption Bands of Pyridine Adsorbed on Solid Acid Catalysts. *J. Catal*., **141**, 347-354.

Ertl, G., H. Knözinger and J. Weoitkamp (1997). *Handbook of heterogeneous catalysis*. (1st ed.). Wiley-VCH, Weinheim (Federal Republic of Germany).

Grasserbauer, M., K. Heinrich and G. Morrison (2009). Nomenclature, symbols and units recommended for in situ microanalysis (Provisional). *Pure Appl. Chem.*, **55**, 2023-2027.

Hall, S. and A. Stocker (2003). API Chemical Synthesis Trends in Reactor System Design. APIs: Reactor Considerations. *The official Journal of ISPE*, **23**, 54-62.

Harris, E. E. and Beglinger, E. (1946). The Madison Wood-Sugar Process, Report no. R1617, US Department of Agriculture, Forest Service, Forest products laboratory, Madison, WI, 1946.

IMM-Catalogue (2007). *The catalogue – process technology of tomorrow*. Institut für Mikrotechnik GmbH, Mainz.

Jansen, J. C., E. J. Creyghton, S. L. Njo, H. van Koningsveld, H. van Bekkum (1997). On the remarkable behaviour of zeolite Beta in acid catalysis. *Catal. Today*, **38**, 205-212.

Jordan, H.-J., R. Brodmann, J. Valentin and M. Grigat (2001). Confocal white light microscopy. World Tribology Congress, 1-4.

Mäki-Arvela, P., T. Salmi, B. Holmbom, S. Willför and D. Yu. Murzin (2011). Synthesis of Sugars by Hydrolysis of Hemicelluloses - A Review. *Chem. Rev.*, **111**, 5638–5666.

Meille, V., S. Pallier and P. Rodriguez (2009). Reproducibility in the preparation of alumina slurries for washcoat application – Role of temperature and particle size distribution. *Colloids and Surfaces A: Physicochem. Eng. Aspects,* **336,** 104–109

Okkerse, C. and H. van Bekkum (1999). From fossil to green. *Green Chem.*, **1**, 107-114.

Paranjpe K. Y (2017). Alpha, Beta and Gamma Alumina as a catalyst - A Review. *Pharma Innovation*, **6**, 236-238.

Rouquerol, J., D. Avnir, C. Fairbridge, D. H. Everett, J. M. Haynes, N. Pernicone, J. D. F. Ramsay, K. S. W. Sing and K. K. Unger (2009). Recommendations for the characterization of porous solids, Technical Report. *Pure Appl. Chem.*, **66**, 1739-1758.

Salmi, T., Mikkola, J. and Wärnå, J. (2011). Toward New Reactor and Reaction Engineering. In: *Chemical reaction engineering and reactor technology*. Boca Raton: CRC Press.

Schmidt, L. D. (2005). *The Engineering of Chemical Reactions* (2nd Edition), Oxford University Press, New York, (U.S.A)

Schmidt, S. A. (2014). Methyl and ethyl chloride synthesis in microreactors. *Ph.D. Thesis*, Åbo Akademi University at Turku/Åbo (Finland).

Silvander, L. General information about the SEM, Johan Gadolin Process Chemistry Centre | Åbo Akademi University.

TechnipFMC, (2017), Ethylene production: a technology leader for grassroots plants and expansions, Ras Laffan, Qatar. Retrieved from https://www.technipfmc.com/en/what-we-do/onshore-offshore/Onshore-capabilities/Ethylene (31/07/19)

Van Haveren, J., E. L. Scott and J. Sanders (2008). Bulk chemicals from biomass. *Biofuels, Bioprod. Bioref*, **2**, 41-57.

Varisli, D., T. Dogu, G. Dogu, (2007). Ethylene and diethyl-ether production by dehydration reaction of ethanol over different heteropolyacid catalysts, *Chem. Eng. Sci.*, **62**, 5349-5352.

Wu, C. Y. and H. S. Wu (2017). Ethylene Formation from Ethanol Dehydration Using ZSM-5 Catalyst. *ACS Omega*, **2**, 4287−4296.

Yue, J. (2018). Multiphase flow processing in microreactors combined with heterogeneous catalysis for efficient and sustainable chemical synthesis. *Catal. Today*, **308**, 3-19.

Zhang, B. (2011). Preparation and characterization of zeolite catalysts based on microreactor elements. *Master thesis in Chemical Engineering,* Department of Chemical Engineering, Åbo Akademi University.

Zhang, M. and Yu, Y. (2013). Dehydration of Ethanol to Ethylene. I*nd. Eng. Chem. Res.*, **52**, 9505-9514.

Zhen, M., F. Zaera (2006). Characterization of Heterogeneous Catalysts. In *Surface and Nanomolecular Catalysis*. Taylor & Francis (CRC Press), 5.

Web sites

https://www.law.cornell.edu/ (last access: 06/09/19)

Acknowledgements

I would like to express my gratitude to Professors Tapio Salmi and Dmitry Murzin, and Docent Narendra Kumar, for the kind and passionate supervision of my master thesis project. I hope someday I will find my way working with the same passion as you do.

Thanks to both Professors Tapio Salmi and Paolo Canu for the help, and for giving me the possibility to take part in this exchange project.

My grateful thanks go to Dr Kari Eränen, being always so patient and supportive, giving me perfect advice and providing the perfect set-up for my experiments.
A huge thank to Professor Johan Wärnå for the help with kinetic simulations, and to Dr Atte Aho for the help with FTIR measurements, filling the dead times with lovely talks about golf and *Italian* dinners.

Coming to Finland, I thought I would find the coldest and darkest place ever, but I was surprised by your warm hospitality. I want to thank all the people from Teknisk Kemi for sharing their knowledge, not only in the field of chemistry: the wide cultural range there helped me filling every day with the joy of discovering something new. Tack så mycket.

A special thanks go to the best friends I could ever found there: Cristina, Lu, Ole, Wander, Sebastian and Matias. For your patience, your listening, your smiles, your jokes, your teasing my weird pronunciatiön; love you all.

Un sentito ringraziamento ai miei amici colleghi – Gaia, Serena, Riccardo e Marco – per la pazienza portata durante questi cinque faticosi anni, per avermi regalato il sorriso ogni giorno di lezione o progetto e per aver reso questo percorso piacevole. Inutile dire che, senza di voi, oggi non sarei qua.

Ai miei amici coinquilini amici – Anna, Sergio, Federico, Elisa e Benedetta – non posso che porgere la mia più sentita gratitudine: per avermi accolta e fatta sentire parte di una nuova famiglia, per avermi insegnato lo studio, l'amicizia e la condivisione, per esserci sempre stati. Il rapporto che abbiamo costruito è qualcosa di molto speciale, e so che lo sarà sempre; non potete neanche immaginare il bene che vi voglio. Una menzione ad Anna per aver corretto questa tesi.

Infinitamente grazie ai miei genitori e a mia sorella, per aver sempre creduto ce l'avrei fatta, per avermi sostenuto emotivamente ed economicamente, ma soprattutto grazie per non aver mai preteso nulla e per non aver insistito di conoscere ogni singola tappa del mio percorso, lasciandomi l'indipendenza a me forse troppo cara. Siete la famiglia migliore che potessi avere.

Alle mie nonne, grazie per l'amore con cui mi avete cresciuta.

Grazie a Debora per aver definito, negli ultimi dieci anni, il mio percorso di studi. Evidentemente, è anche a questo che servono gli amici.

Un ringraziamento agli amici che mi hanno accompagnato in questi anni, in particolare Samuele, Monica, Carlotta, Davide, Alice. Ognuno di voi ha, a suo modo, contribuito a rendere me la persona che sono oggi.

Finalmente, Matteo, grazie. Per tutta la tranquillità e l'amore che mi trasmetti.

"Ho diciotto anni e già la felicità ha il sapore della memoria."